2

CR-128543

MASSACHUSETTS INSTITUTE OF TECHNOLOGY

APOLLO

GUIDANCE, NAVIGATION AND CONTROL

MIT

CHARLES STARK DRAPER LABORATORY

CAMBRIDGE MASSACHUSETTS 02139

MASSACHUSETTS INSTITUTE OF TECHNOLOGY

APOLLO

GUIDANCE, NAVIGATION AND CONTROL

Approved: Donald C Fraser Date: 31 July 1972
D. C. FRASER, DIRECTOR, CONTROL AND FLIGHT DYNAMICS
APOLLO GUIDANCE AND NAVIGATION PROGRAM

Approved: Stephen L. Copps Date: 31 July 1972
S. L. COPPS, COLOSSUS PROJECT MANAGER
APOLLO GUIDANCE AND NAVIGATION PROGRAM

Approved: R. H. Battin Date: 31 July 1972
R. H. BATTIN, DIRECTOR, MISSION DEVELOPMENT
APOLLO GUIDANCE AND NAVIGATION PROGRAM

Approved: David G. Hoag Date: 1 Aug 72
D. G. HOAG, DIRECTOR
APOLLO GUIDANCE AND NAVIGATION PROGRAM

Approved: D. G. Hoag for Date: 1 Aug 72
R. R. RAGAN, DEPUTY DIRECTOR
CHARLES STARK DRAPER LABORATORY

E-2704

CSM DOCKED DAP/ORBITAL ASSEMBLY BENDING INTERACTION—AXIAL CASE—FINAL REPORT

July 1972

MIT CHARLES STARK DRAPER LABORATORY
CAMBRIDGE, MASSACHUSETTS, 02139

ACKNOWLEDGEMENT

This report was prepared under DSR Project 55-23890, sponsored by the Manned Spacecraft Center of the National Aeronautics and Space Administration through Contract NAS 9-4065.

E-2704

CSM DOCKED DAP/ORBITAL ASSEMBLY BENDING INTERACTION—AXIAL CASE—FINAL REPORT

Abstract

As part of its involvement with the SKYLAB project, the Draper Laboratory designed a digital autopilot which can provide attitude control for the entire SKYLAB Orbital Assembly using the Service Module reaction control jets. An important consideration was the potential interaction of the control system with the bending modes of the Orbital Assembly. Two aspects of this potential interaction were considered. The first was the possibility that bending induced rotations feeding back through the attitude sensor into the control system could produce an instability or self-sustained oscillation. The second was whether the jet activity commanded by the control system could produce excessive loads at any of the critical load points of the Orbital Assembly. Both aspects were studied by using analytic techniques and by running simulations on the MIT all-digital simulator.

This report elaborates on the problem itself, the techniques used to investigate the problem, and the results of the investigation. The reader who is pressed for time is referred to the Summary and Conclusions section. Those interested in the techniques used in the investigation, and in the assumptions made in conjunction with those techniques are encouraged to read the report in its entirety.

by

Joseph F. Turnbull
and James E. Jones

July 1972

TABLE OF CONTENTS

LIST OF ILLUSTRATIONS

LIST OF TABLES

I. Introduction

This report documents the investigations into the interaction between the CSM Docked DAP and the bending modes of the SKYLAB Orbital Assembly in its nominal docked configuration (designated Configuration 1.2). This configuration, shown in Fig. 1, consists of one CSM docked with the Orbital Workshop in the axial port of the Multiple Docking Adapter.

The bending interaction investigation has two distinct parts:

1. the study of the influence of bending on DAP control, and
2. the study of the magnitude of loads induced by DAP-commanded RCS-jet activity at various critical load points.

Figures 2a and 2b illustrate the investigation's two parts. Both figures show a conceptual diagram of the DAP/flexible vehicle system. Jet-firings occur in response to DAP commands. These firings cause changes in the attitude of the vehicle, θ_{RB}, that can be described by rigid body dynamical equations of motion. In addition, the jet activity excites the bending modes of the vehicle. The excited bending modes produce both loads and flexure throughout the vehicle. The sum of rigid body rotation and bending rotation at the IMU station is the indicated vehicle attitude sensed by the Inertial Measurement Unit. The DAP's estimate of attitude and attitude rate is derived from the IMU's measurement of θ_{total}.

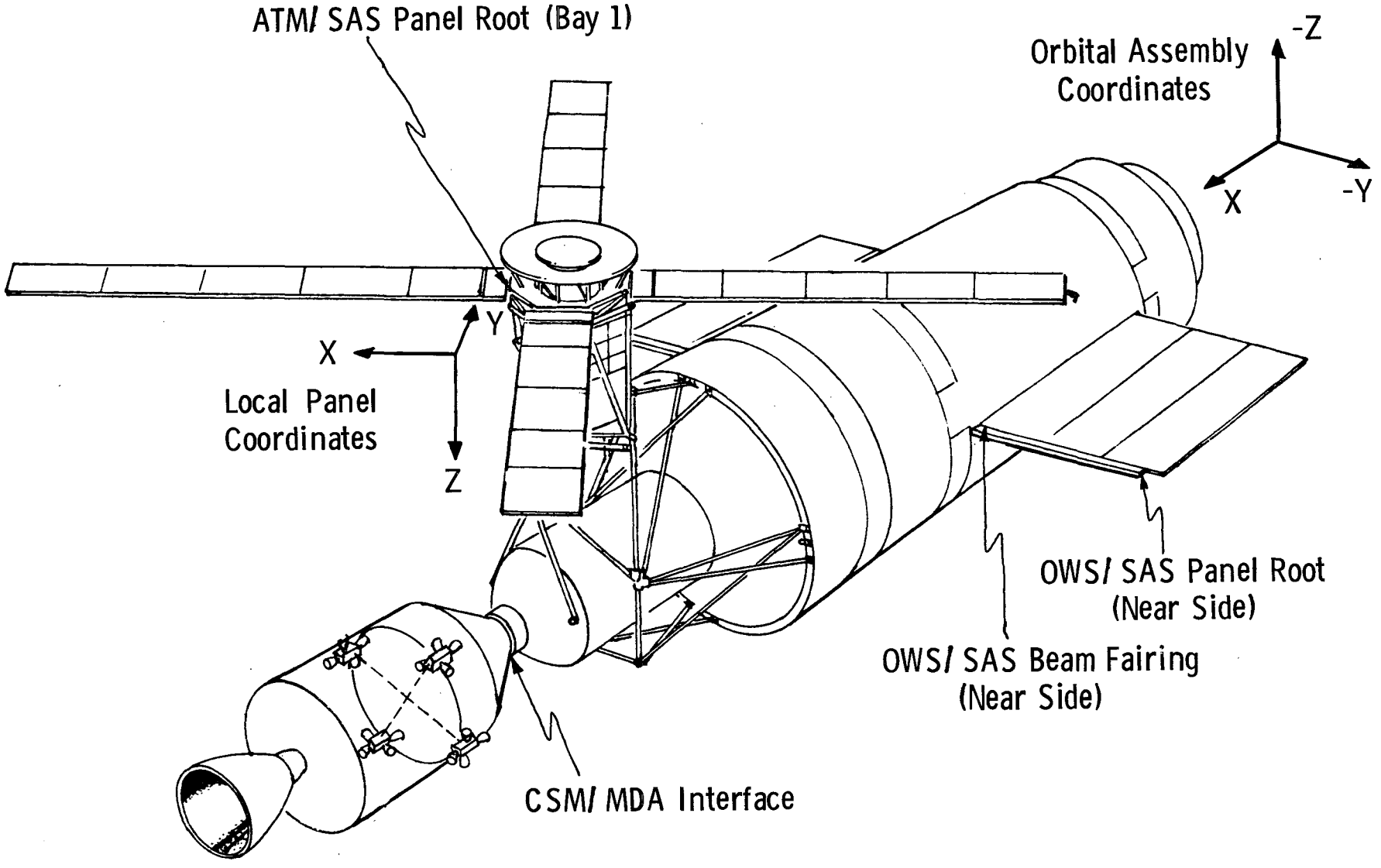

Fig. 1 Nominal Docked Configuration With Load Points Shown

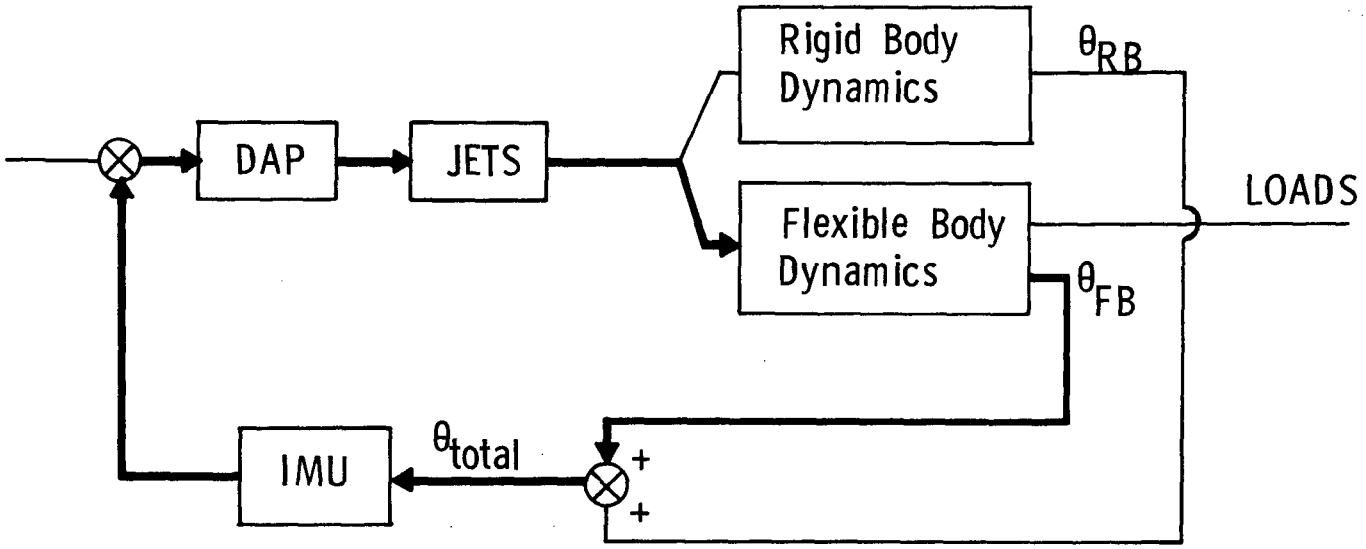

Fig. 2a System Diagram with Emphasis on Closed Loop DAP/Bending Mode Interaction

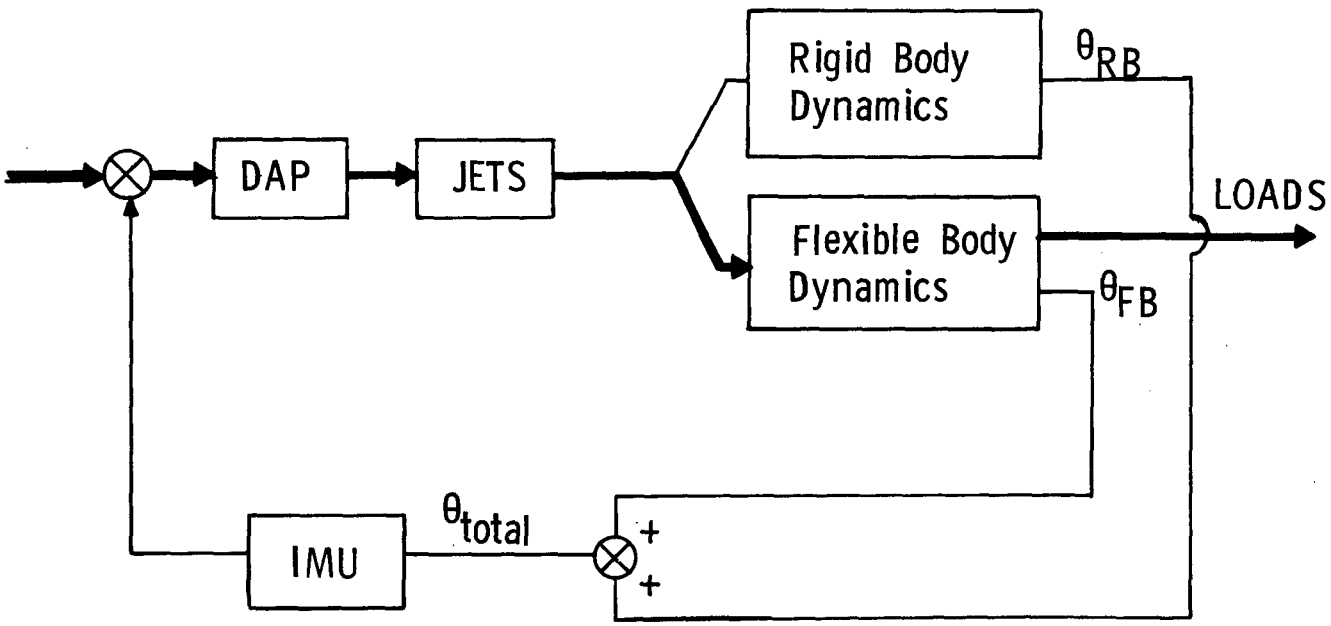

Fig. 2b System Diagram with Emphasis on the Load Inducement Part of the Investigations

Part I of the investigation examines the closed loop interaction indicated by the heavy lines in Figure 2a. The bending flexure, θ_{FB}, can be "read" by the IMU. In turn, the DAP can respond to this "reading" by firing jets. Conceivably, these firings can reinforce the bending already in progress. This part of the investigation considers the likelihood that such potential reinforcement will result in a bending instability or a self-sustained bending oscillation.

The heavy lines of Fig. 2b are intended to show that the emphasis in Part 2 of the investigation is on observing the loads that result from various types of DAP activity (e.g., translation, attitude hold against disturbances, etc.). To be sure, the feedback paths are included in DAP simulations, however, the point is that Part 2 does not concentrate on the feedback mechanism but rather on observed loads. In summary, the concern of Part 2 can be phrased as a question: Does the normal jet activity commanded by the DAP when maneuvering and holding attitude against disturbances result in excessive bending loads?

Each part of the investigation has been treated from a theoretical point of view using the results of an analytic worst-case study. The nature of the worst-case study and the assumptions made in carrying it out are discussed briefly in the next section.

To provide support for the theoretical treatment, specific simulations have been run in conjunction with each of the investigation's two parts. These simulations were performed on the MIT all-digital simulator. This simulator duplicates in a bit-by-bit fashion the functioning of the DAP and, for that matter, of the whole Apollo Guidance Computer. It also simulates the operation of the Inertial Measurement Unit and the dynamics of the entire vehicle including 92 flexible body modes for the Orbital Assembly.

Both the worst-case study and the all-digital simulator use bending data supplied by Martin Marietta Corporation. The data is supplied in the form of modal frequencies, generalized bending displacements at the RCS quads, generalized rotational deflections at the Navigation Base, and matrices which transform computed modal accelerations and static RCS forces into moment loads at the selected load points listed in Table 1 and shown in Fig. 1. The data, dated January 1972, differs from previous versions by the recent revision (downward) of OWS/SAS panel stiffness.

Table 1: Load Point Descriptions, Configuration 1.2

Load Point	Load Station (Launch Vehicle Coordinates) (Inches) X	Y	Z
CSM/MDA Interface	3650.0	0.0	0.0
ATM/SAS Panel Root (Bay 1)	(Local Coordinates 0, 0, 0)		
OWS/SAS Beam Fairing (Near Side)	3172.4	-124.6	-61.7
OWS/SAS Panel Root (Near Side, Outboard)	3175.5	-478.5	-53.1

As mentioned above, the next section of this memo is a brief discussion of the worst-case study. Following it are four sections that discuss each part of the investigation from both the theoretical and simulation points of view. The ordering of the sections is:

Section III Closed loop interaction – theoretical considerations

Section IV Closed loop interaction – simulation support

Section V Load inducement – theoretical considerations

Section VI Load inducement - simulation support

Observations and conclusions constitute the final section of this report. It is found that highest ratio of induced load to load limit can be expected to occur about the X axis at the CSM/MDA interface. One simulation, in fact, shows a peak load of 72,470 in-lb which is 83% of the limit. While it is impossible to guarantee that no CSM/MDA X-axis load will ever exceed 72,470 in-lb, reasons are brought out for viewing this value as a pessimistic result. The ultimate conclusion of the final section and of the memo as a whole is that the CSM Docked DAP as it exists in SKYLARK I can be expected to execute any maneuvers it is called upon to perform without resulting in a bending instability or inducing excessive loads.

II. Worst-Case Analysis

The results of the worst-case analysis technique are used in subsequent sections to verify that the DAP does not sustain or strongly reinforce bending via oscillations perceived at the CSM IMU location and to identify for detailed study those situations where high loads may be induced by DAP activity. Appendix A of this memo is a reproduction of Appendix A of SKYLARK Memo #51 and is a detailed discussion of the linear worst-case analysis technique.

In brief, the worst-case analysis examines bending-induced rotational deflections at the CSM IMU location and moment loads at the selected stations when the excitation due to jet activity approximates the theoretical worst case. The theoretical worst-case forcing function for any one jet is a square wave in which the jet is alternatively "on" and "off" for equal periods of time. The basic assumptions made in conducting the worst-case analysis are:

1. The jet on-off square wave excitation is modeled by a sinusoid because, in the Fourier series representation of the output, contributions from frequency components higher than the fundamental are found to be negligible.

2. Each mode is excited separately at resonance. Consequently, the additive effects of adjacent modes are lost, but these effects are small because the low damping associated with the bending modes yields very sharp resonance peaks. Thus, the amplification factor associated with an adjacent mode being excited at near-resonance is small compared with the amplification factor of the mode being excited at resonance, * even when the frequency separation of the two modes is very small.

3. A single-jet excitation is assumed, but in analyzing the data of worst-case study, the effects of those jets which can fire synchronously are summed to yield the worst-case outputs.

---

* Comparison of the results of the worst-case analysis with a frequency response analysis done by Martin Marietta in which all modes are excited simultaneously by a sinusoid at a particular forcing frequency indicates that neglecting the effects of adjacent modes is valid.

4. A damping ratio of 0.01 is assumed. This value is used to be consistent with Martin Marietta's frequency response analysis. However, bending rotational deflections and moment loads which approach only half of assumed limits are flagged out to account for the fact that a damping ratio of 0.005* would produce resonant amplitudes and loads twice as high as for 0.01.

5. Only steady-state oscillations are considered.

6. Loading due to rigid-body rotational acceleration is neglected.

Of course, the simplifying assumptions listed above apply only to the worst-case analysis; these assumptions are not used in the M.I.T. all-digital simulator.

---

* The M.I.T. all-digital simulator uses the pessimistic value 0.005 for modal damping ratio. (A damping ratio of 0.01 ± 0.005 is recommended by the data source.)

III. Closed Loop Interaction – Theoretical Considerations

The theoretical approach to the question of closed loop interaction uses the worst-case study in the following way. Among the results of the worst-case study are the steady-state peak-to-peak amplitudes of rotational deflections at the CSM IMU location that result from periodic excitation by the jets at the natural frequency of each bending mode. The worst-case study calculates analytically the peak-to-peak amplitude of the rotational deflection for each mode/jet combination. Since it is possible to command two jets synchronously, the effects of the two jets which include the largest rotational deflections are summed for each mode.

The six modes which exhibit the largest summed amplitudes* are listed in Table 2. The first column of the table gives the frequency of the mode. The second column gives the name or description of the mode. The third column gives the value of the summed peak-to-peak amplitude of rotation at the navigation base. The fourth column will be discussed just a little later. The largest of all these peak-to-peak resonant amplitudes is 0.410 deg. which occurs when the first CSM axial mode (natural frequency = 1.226 cps) is excited at resonance by jets 10 and 12. The significance of this is understood when referenced to the phase plane used by the control logic segment of the DAP. This phase plane is shown in Fig. 3. The DAP deadband is the half-width of the phase-plane drift-zone. It is expected that the normal minimum deadband used during DAP operation will be 0.5 deg. This means that the full width of the phase-plane drift zone will usually be a degree or more. A stability problem could arise if the amplitude of oscillation at the CSM IMU due to bending was so large that the phase point was alternately outside the drift-zone to the right with a resulting negative firing being commanded and then outside the phase plane to the left with a resulting positive firing. Activity of this sort could reinforce the bending state or at least sustain the bending oscillation. However,

---

* Other modes yielded much smaller worst-case rotations.

Excitation Frequency (cps)	Primary Contributing Mode	"Measured" Attitude Oscillation (p-p, in deg)	"Filtered" Rate Oscillation (p-p, in deg/sec)
0.205	First ATM/SA Bay 1	0.356	0.043
0.383	First OWS/SA (Near Side)	0.184	0.013
1.226	First CSM (Axial)	0.410	0.010
1.368	Second CSM (Axial)	0.358	0.008
2.381	Fifth ATM/DA	0.122	0.002
2.966	Third CSM (Axial)	0.226	0.004

Table 2: Six Largest Peak-to-peak Attitude and Rate Oscillations for Worst-case Analysis of Configuration 1.2

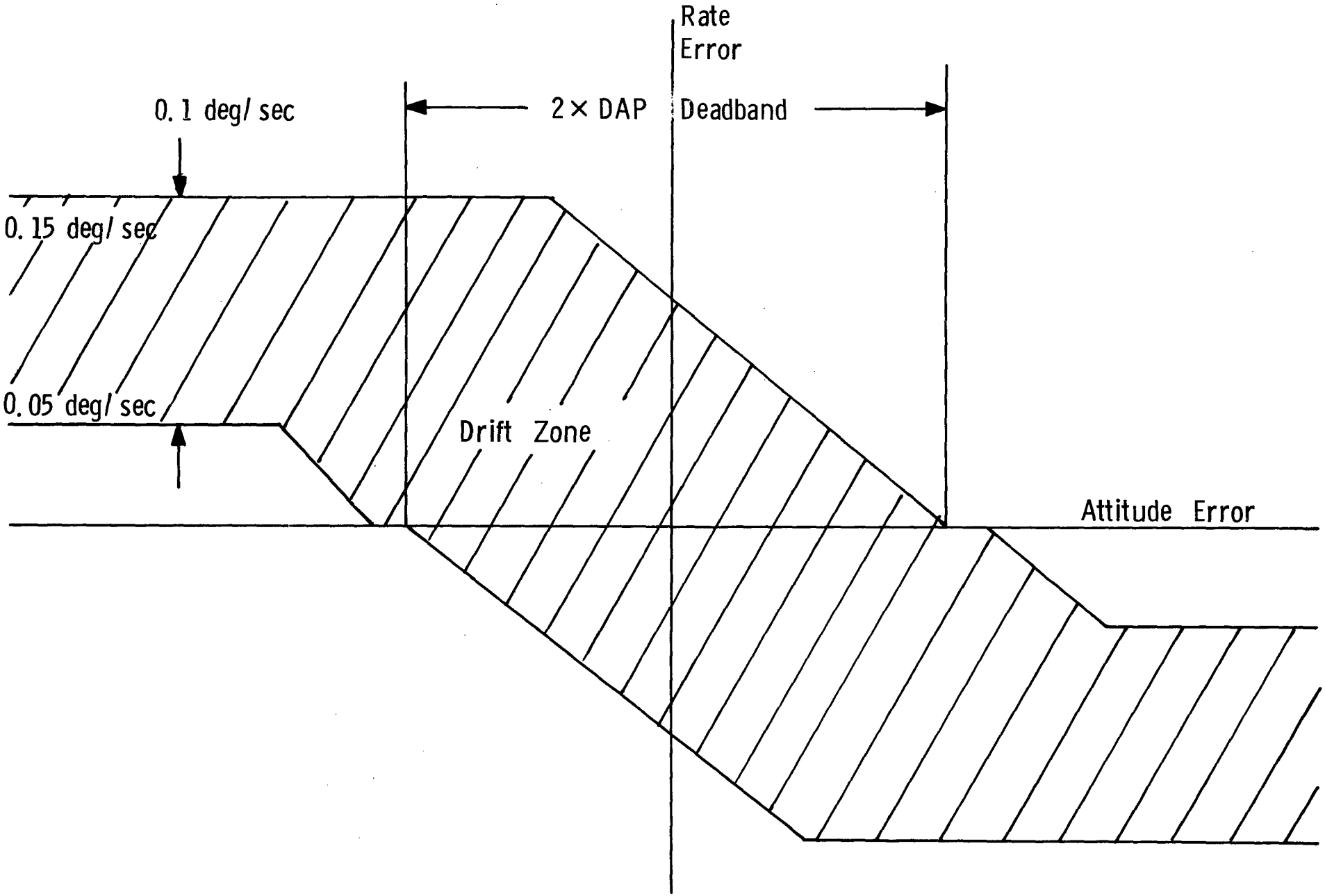

Fig. 3 CSM-Docked DAP Phase Plane

in light of the peak-to-peak amplitudes listed in Table 2, the following statement can be made. Even if the vehicle bending modes are somehow excited to a level that produces rotational oscillations at the CSM IMU location equal to the maximum value shown in Table 2, that amplitude of rotation would be too small to produce self-sustaining jet activity resulting from the phase point alternately falling to the right and left of the drift-zone.

The above statement does not completely cover the theoretical consideration of closed loop interaction for it considers only the horizontal motion of the phase point. The vertical position of the phase point is the difference between estimated rate and commanded rate. During any maneuver and of course during attitude hold, commanded rate will be constant. Estimated rate, however, is the output of a second-order filter that uses attitude measurements as an input. Thus, in general, an oscillatory attitude input will result in an oscillatory rate-estimate output. The peak-to-peak amplitude of this output can be predicted analytically. The appendix of "Analysis of SKYLAB Docked-DAP Angular Rate Filter" (SKYLARK Memo #61) describes in some detail the derivation of the analytic expression that can be used for this purpose. This analytic expression has been applied to the six cases enumerated in Table 2. The results are listed in the fourth column of that table. The maximum peak-to-peak amplitude listed in column four is 0.043 deg/sec. Since the vertical dimension of the phase plane drift zone shown in Fig. 3 is 0.1 deg/sec or greater, the following statement can be made. Even if the vehicle bending modes are somehow excited to the levels induced by worst-case jet excitation, the resulting oscillation in rate estimate will be too small to produce self-sustaining jet activity resulting from the phase point alternately falling above and then below the drift-zone.

IV. Closed Loop Interaction - Simulation Support

Supporting evidence that the DAP does not sustain bending oscillations is provided by two simulations that were specifically addressed to the question of closed loop interaction. In each simulation the DAP is turned on shortly after one of the modes listed in Table 2 is artifically given a large initial amplitude. In the first case, the 1.226 cps mode is given an initial condition that results in a 1.2 deg angular rotation about the Y CSM control axis at the CSM IMU location. Figure 4 shows the jet-firing history which occurred. No maneuvering is in progress and there are no disturbance torques being applied during this simulation. The jet acitivity is directly attributable to the very high* amplitude bending that has been artificially induced. The firing pattern indicates that jets are not being commanded synchronously with the 1.226 cps mode. Figure 5, which shows the time history of the rotational deflection about the CSM Y axis at the CSM/IMU station, confirms that the natural damping of the mode is not noticably affected by the jet activity. Quantitatively, with a damping ratio of 0.01, the envelope of the oscillation would be expected to reduce from an initial value of 1.2 deg to 0.098 deg after 65 seconds. In the simulation the observed value of the envelope at 65 seconds is 0.1 deg

In the second case, the 0.205 cps mode is given an initial 0.75 deg† angular deflection about the CSM X axis. Figure 6 shows the jet-firing history which is induced. Initially, the jets fire in synchronization with the mode; eventually, however, the firing pattern becomes irregular. Figure 7 indicates that the amount of energy added to the 0.205 cps mode by the synchronous jet-firings is not significant. The mode damps naturally as in the previous case.

Since these simulations show that the DAP will not even sustain bending modes that artifically have been given deflections that exceed the phase plane drift zones, then there should be no concern that the DAP will generate a self-sustained oscillation of its own.

---

* The bending oscillation starts with a peak-to-peak amplitude of 2.4 deg which is more than four times the worst peak-to-peak amplitude listed in Table 2.

† 1.5 deg peak-to-peak

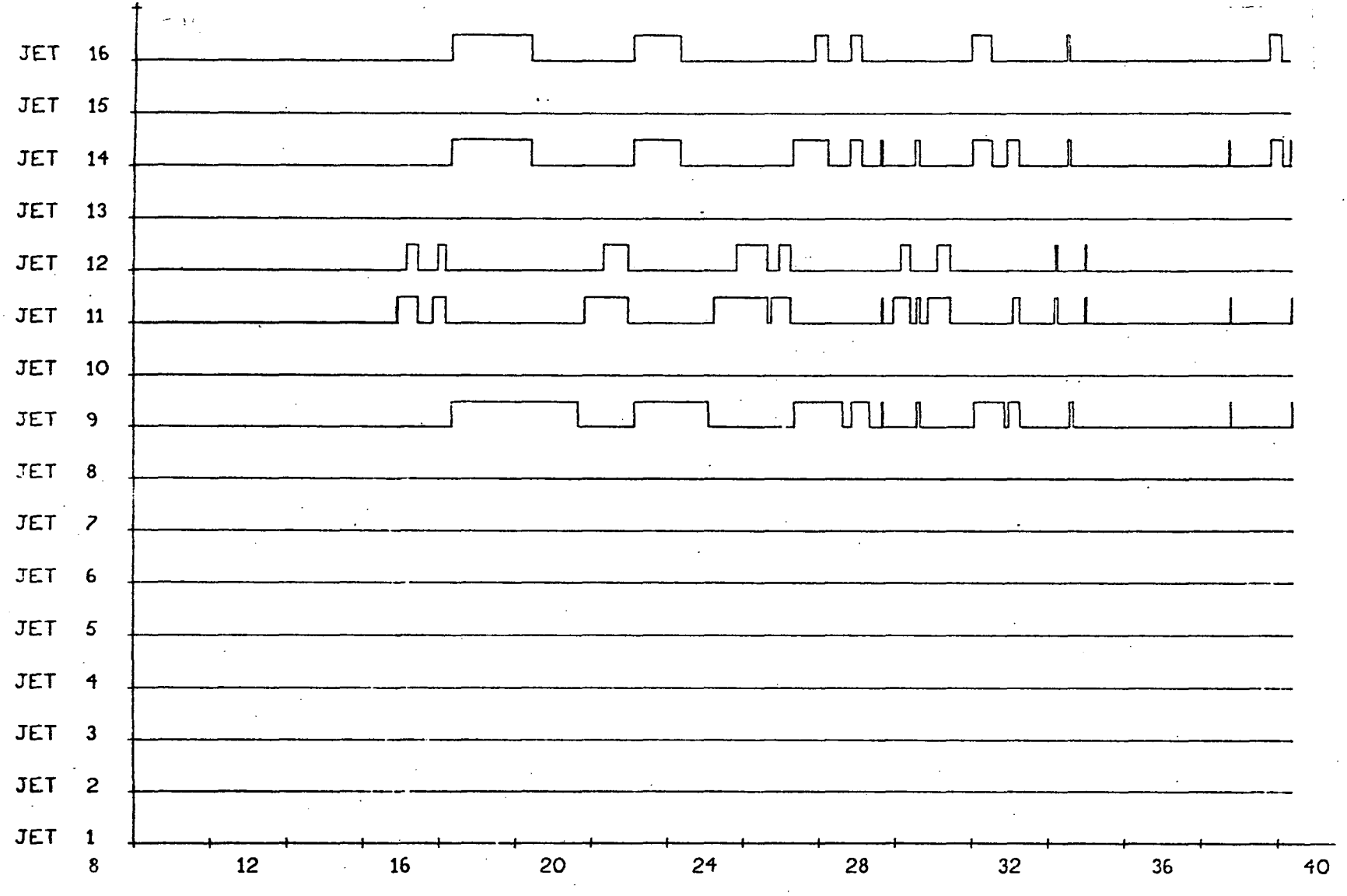

Fig. 4 Jet-firing History for Case with Initial 1.2 Degree Rotational Deflection

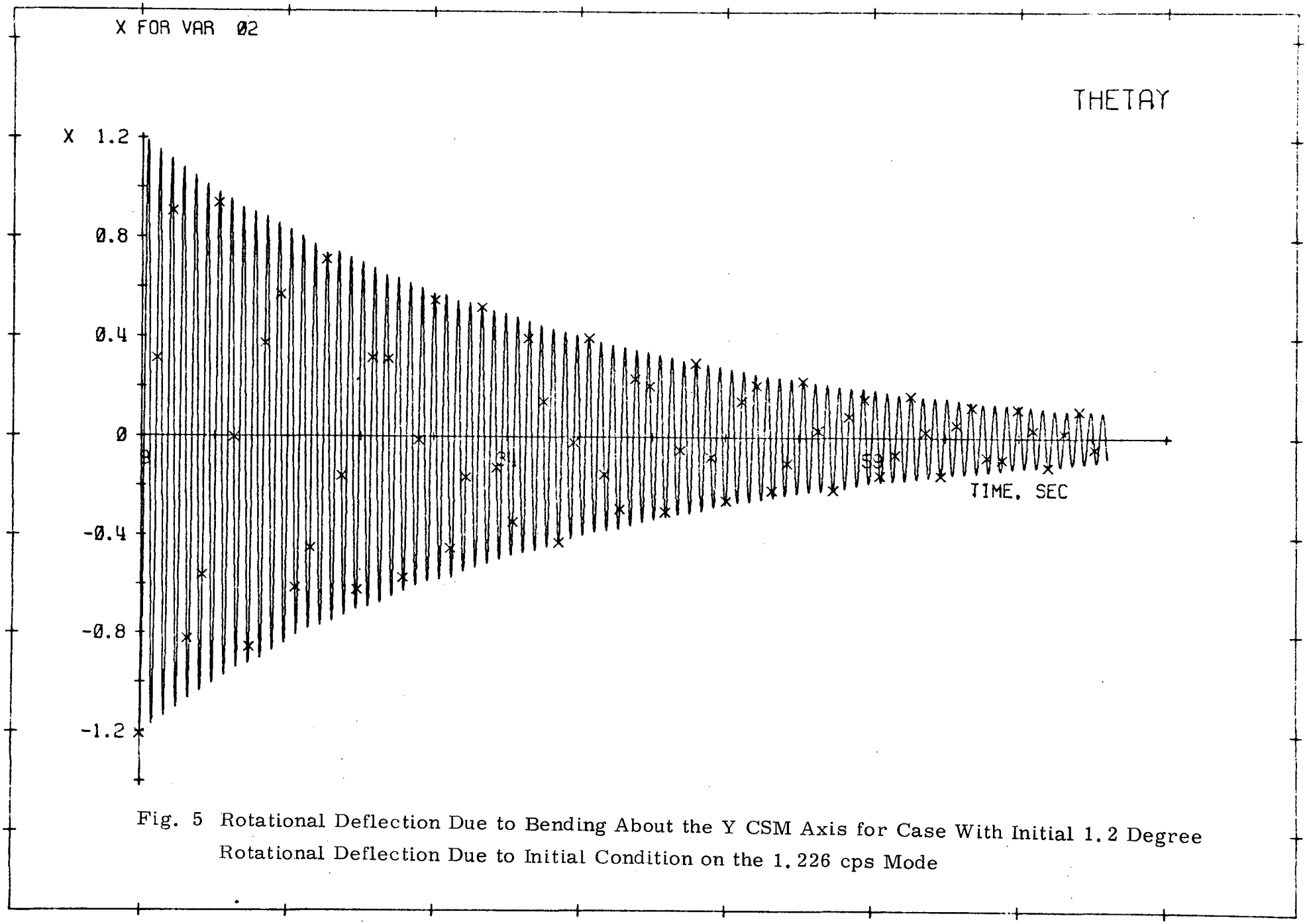

Fig. 5 Rotational Deflection Due to Bending About the Y CSM Axis for Case With Initial 1.2 Degree Rotational Deflection Due to Initial Condition on the 1.226 cps Mode

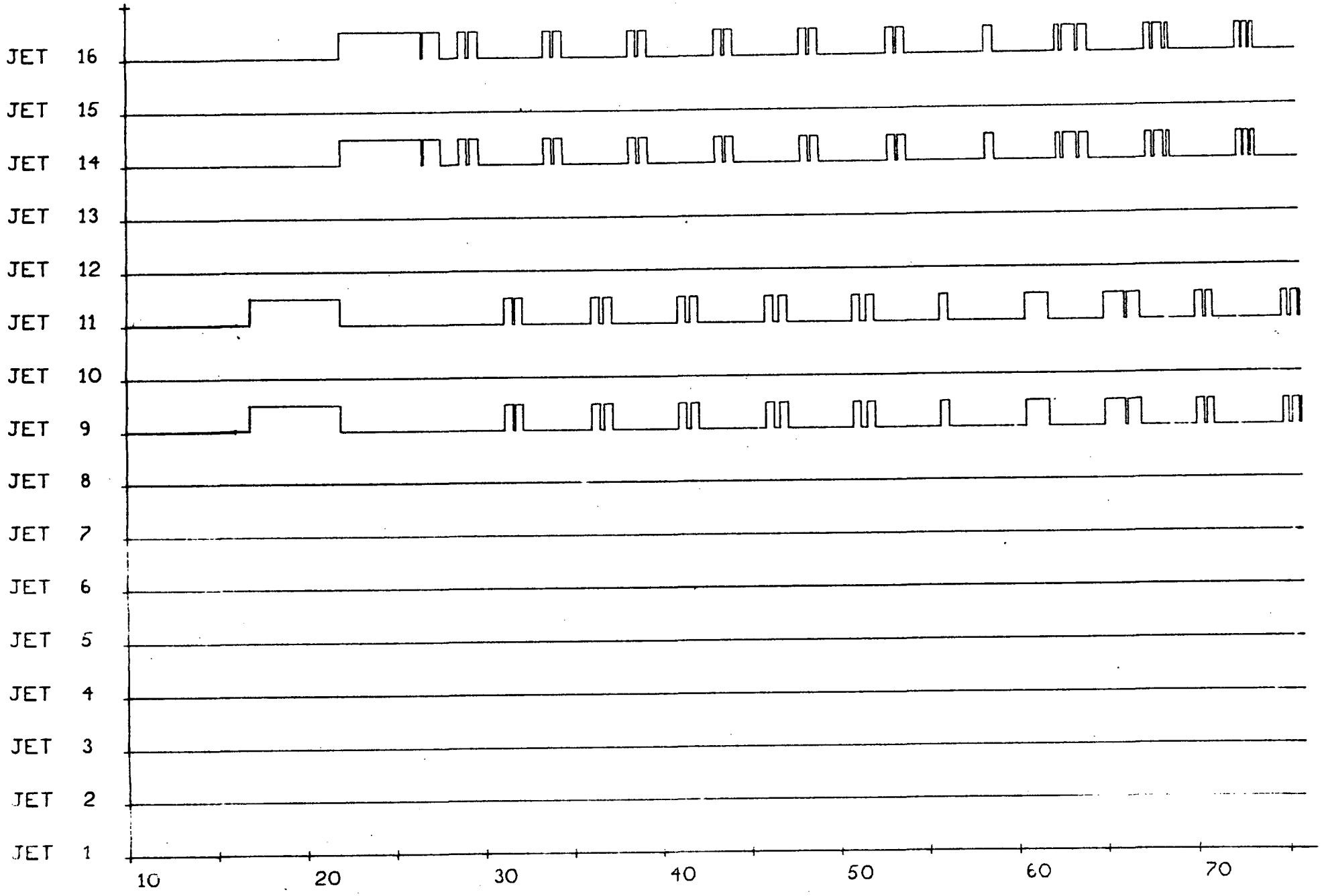

Fig. 6 Jet-firing History for Case With Initial 0.75 Degree Rotational Deflection Due to Initial Condition on the 0.205 cps Mode

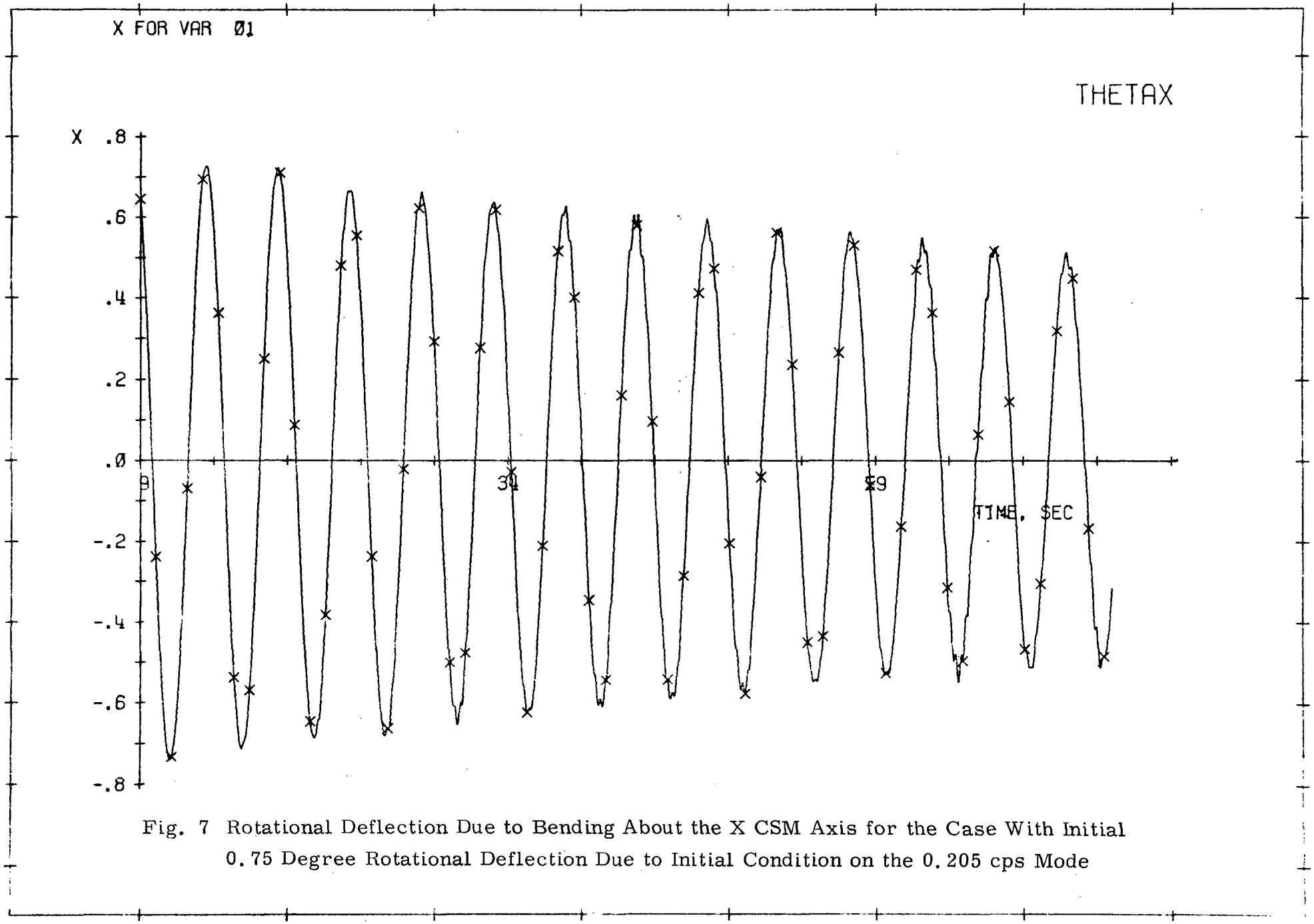

Fig. 7 Rotational Deflection Due to Bending About the X CSM Axis for the Case With Initial 0.75 Degree Rotational Deflection Due to Initial Condition on the 0.205 cps Mode

V. Load Inducement - Theoretical Considerations

The second part of the worst-case study is the calculation of loads produced at various critical points as a result of the resonant excitation of each of the modes by each of the jets in turn. The critical points are places of load concentration which might exhibit loading that is high relative to the strength capability at that point. The load points examined in the worst-case study and also in the simulations discussed in the next section are indicated in Fig. 1 and are listed in Table 1 of the introductory section.

Of central importance to the study of load inducement is the question of load limits. For each load point, three limits are given in Table 3. These are the limits for moment load about the X, Y and Z axis at the point. For all points except the ATM/SAS point, the axes are parallel to the Orbital Assembly axes (cf Fig. 1). For the ATM/SAS point, a local coordinate frame is used. The X axis of the local frame is parallel to the long dimension of the solar array. The Z axis is normal to the solar array elements. The Y axis completes a right-hand coordinate frame. The local frame for the Bay 1 solar array is shown in Fig. 1.

Table 3 lists the load limit values upon which the conclusions of this report are based. The CSM/MDA M_x, M_y and M_z; ATM/SAS M_x, M_y and M_z; and OWS/SAS/BF M_x and M_y values are based on Table III of the Marshall Space Flight Center report, "Cluster Orbital Maneuver Loads."* The CSM/MDA M_x limit ultimately turns out to be the most critical limit because it is there that the ratio of observed loads during simulation to load limit is the highest. The 88,000 in-lb value quoted in the MSFC document is

---

* Sterett: "Cluster Orbital Maneuver Loads", S & E - ASTN - ADL (71 - 96).

Load Station and Axis			Load Limit
Static	M_X	CSM/MDA	
Dynamic	M_X	CSM/MDA	
Total	M_X	CSM/MDA	88,000
	M_Y	CSM/MDA	600,000
	M_Z	CSM/MDA	600,000
	M_X	ATM/SAS	9,006
	M_Y	ATM/SAS	44,100
	M_Z	ATM/SAS	130,800
	M_X	OWS/SAS/BF	83,000
	M_Y	OWS/SAS/BF	35,000
	M_Z	OWS/SAS/BF	28,700
	M_X	OWS/SAS/PR	1,000
	M_Y	OWS/SAS/PR	17,000
	M_Z	OWS/SAS/PR	26,350

Table 3. Load Limit Values Used in Evaluating Results of the Study's Load Inducement Part

ultimately based on a North American Rockwell I. C. D. * The I. C. D. actually states a limit value of 82, 100 in-lb. It is our understanding that NAR uses a safety factor of 1. 5 in arriving at the 82, 100 in-lb value but that MSFC assumes a 1. 4 safety factor and thus arrives at a load limit of 88, 000 in-lb.

The OWS/SAS/BF M_z and OWS/SAS/PR M_x, M_y and M_z values are based on Table VI of "Orbital Maneuver Loads Report (Final)"** issued by the Martin Marietta Corporation. The cited MSFC report states a limit value of 33, 000 in-lb for M_z at the OWS/SAS/BF point. For the sake of caution, however, the 28, 700 in-lb value of the Martin document was used in Table 3 of this Draper Lab report.

The aim of the load inducement phase of the worst-case study is to identify which bending modes, when excited at resonance, will produce significant loads at one or more of the load points. Table 4 lists the cases where, when the effects of pairs of jets that can fire together are summed, the resulting load exceeds 50%*** of the limit value.

As discussed in Section II, the assumed excitation is a worst-case half-cycle-on, half-cycle-off jet activity pattern. In practive, however, it is highly unlikely that jet-firing sequences which resemble the worst-case square-wave input will be commanded. Regular (but not truly periodic) jet-firing sequences are commanded only when the DAP is holding against disturbance accelerations. Variations in the disturbances, non-linearities in the phase-plane, and computer quantization and truncation all serve to disrupt the periodicity of these jet-firing sequences. In addition to this inherent randomness

---

* Interface Control Document #13MO4632, "CSM to MDA AAP Functional and Proceedural Requirements for Missions AAP 1, 2, 3 and 4", original issue 1/7/70, revision 5 6/23/71.

**Singh, Jay N. and Heath, Robert A. ; "Orbital Maneuver Loads Report (Final)", Martin Marietta Corporation-Denver Division, 19, Nov. 1971, ED - 2002 - 1281 - 2.

*** As mentioned above, the factor of 50% is used to account for the fact that a 0. 01 damping ratio is used in the worst-case study and that if the damping ratio were at the low end of the predicted range (0. 005), the resonant loads would be twice those for 0. 01 damping.

Station	OA Axis	Freq (cps)	Jet Pair	Load (in-lb)	Assumed Limit
CSM/MDA	X	2.381	(9, 11)	64,400	88,000
"	"	"	(14, 16)	63,100	"
"	"	2.966	(9, 11)	272,000	"
"	"	"	(14, 16)	266,000	"
"	"	3.017	(9, 11)	92,400	"
"	"	"	(14, 16)	90,500	"
CSM/MDA	Y	1.226	(11, 12)	346,000	600,000
ATM/SAS	Z	2.932	(11, 12)	85,500	130,800
"	"	"	(15, 16)	86,200	"
"	"	2.966	(11, 12)	104,800	"
"	"	"	(15, 16)	105,700	"
OWS/SAS/BF	Z	0.562	(11, 12)	24,400	28,700
"	"	"	(15, 16)	41,700	"
"	"	1.196	(11, 12)	44,600	"
"	"	"	(15, 16)	43,900	"
OWS/SAS/PR	Y	0.383	(11, 12)	5,400	8,500*
"	"	"	(15, 16)	5,400	"

*Since this part of the study was conducted, this assumed limit has been revised upward to 17,000 (cf Table 3.)

Table 4. Worst-Case Analysis Load Values for Combined Jets that Exceed 50% of Table 3 Limits

observed in firing frequencies, pulse widths are also random and in general differ substantially from the half-period pulse associated with square wave excitation assumed in the worst-case study. Appendix B shows the derivation of a reduction factor that can be applied to entries in Table 4 to predict the load produced by a pulse train that is periodic and in resonance with the mode being considered but that has the jet on for other than a half-cycle.

Taking into account the above practical considerations, several of the entries in Table 4 can be eliminated from further consideration. Table 5 enumerates the cases that remain. The significance of Table 5 and indeed of the whole load inducement phase of the worst-case study is not that the load point/mode / jet pair combinations designated there are likely to cause a problem. Rather the interpretation is that if a problem does arise it is most likely to arise

1. at the CSM/MDA load point about the X axis due to exciting the 2.966 cps mode,
2. at the OWS/SAS/BF load point about the Z axis due to exciting either the 0.562 cps or 1.196 cps mode, or
3. at the OWS/SAS/PR load point about the Y axis due to exciting the 0.383 cps mode.

Station	OA Axis	Freq (cps)	Jet Pairs
CSM/MDA	X	2.966	(9, 11), (14, 16)
OWS/SAS/BF	Z	0.562, 1.196	(11, 12), (15, 16)
OWS/SAS/PR	Y	0.383	(11, 12), (15, 16)

Table 5. Load Point Cases that Deserve Close Scrutiny

VI. Load Inducement - Simulation Support

In a project like SKYLAB, simulation must take the place of flight testing. The MIT all-digital simulator, developed over the years in support of the Apollo project, offers a high-fidelity representation of the onboard subsystems (computer, inertial measurement unit, etc.) as well as of the rotational and translational dynamics of the spacecraft. In addition, for SKYLAB, the capability of simulating 92 flexible body bending modes has been added to the simulator.

A number of test sequences have been devised that expose the Docked DAP to the range of maneuver environments that it might be exposed to during a mission. Test sequences include rotation and translation maneuvers. Disturbance torques applied during some of the tests ranged from torques on the order of gravity gradient disturbances to torques resulting from jet on-failures. Table 6 defines the tests that are reported in this memo. The quantitative results contained in this memo are from simulations that were performed using the mode and load data dated January 1972. These data are the most current and are considered to be the best available. Simulations of the types enumerated in Table 6 have been run on data of other vintages. The results of those simulations have the same general character as the results reported herein. This fact increases our confidence in making generalizations based on the seven simulations reported here. Numerical results of these earlier simulations, however, are not presented in this memo because the mode and load data is now outdated and also because the addition of more columns of numbers to the Table of results might submerge in a mass of data the important points to be made.

While each test sequence of Table 6 was being performed, an automatic edit program monitored the loads about each axis at the four critical points. At the end of the simulation, the edit program printed the maximum load observed during the simulation. The magnitudes of these maximum values are tabulated for each case in Table 7. For convenience, the first column of the table reproduces the

Table 6. Simulation Cases for Load-Inducement Part of Study

CASE 1	Initial rates and torques during simulation chosen so as to produce several small firings during the sim like those that would occur during Attitude Hold against gravity gradient torque. Bending mode damping ratio set to $\zeta = 0.005$.
CASE 2	Automatic maneuver at 0.2 deg/sec from initial gimbal angles 0, 0, 0 degrees to final gimbal angles 5, 5, 5 degrees Bending mode damping ratio set to $\zeta = 0.01$.
CASE 3	Initial roll rate, +X translation beginning at T = 20 sec, 6.77 newton-meter roll disturbance torque beginning at 30 sec. Bending mode damping ratio set to $\zeta = 0.005$.
CASE 4	X translation beginning at 20 sec. Jet 15 in failed-on condition between 40 and 60 sec. Bending mode damping ratio set to $\zeta = 0.005$.
CASE 5	CASE 4 rerun with bending mode damping ratio changed to $\zeta = 0.01$.
CASE 6	CASE 4 rerun with a different set of DAP constants (see text for description of the change in constants). Bending mode damping ratio set to $\zeta = 0.005$.
CASE 7	On failure of Jet 15 during attitude hold (no X translation). DAP constants of CASE 6 used. Bending mode damping ratio set to $\zeta = 0.005$.

assumed load-limit information of Table 3.

The CSM/MDA load point differs from the other load points in that both a static and a dynamic load are calculated for each of the axes at that point. The static load is the load that exists as direct result of the jets applying torque to the Orbital Workshop through the docking

Table 7. Load Maxima During Simulation *

			Load Limit	CASE 1	CASE 2	CASE 3	CASE 4	CASE 5	CASE 6	CASE 7
Static	M_X	CSM/MDA		7,844	15,102	14,921	15,664	15,664	15,664	15,484
Dynamic	M_X	CSM/MDA		10,188	27,824	38,060	66,479	43,394	61,156	58,290
Total	M_X	CSM/MDA	88,000	3,707	27,824	37,936	72,470†	47,439	65,844	58,379
	M_Y	CSM/MDA	600,000	8,423	23,531	93,902	57,315	46,786	67,135	28,810
	M_Z	CSM/MDA	600,000	9,134	44,574	76,972	55,183	37,736	57,734	32,236
	M_X	ATM/SAS	9,006	15	63	129	136	148	204	236
	M_Y	ATM/SAS	44,100	442	550	1,388	1,551	1,258	1,074	1,022
	M_Z	ATM/SAS	130,800	885	3,258	9,161	11,346	9,196	14,464	18,272
	M_X	OWS/SAS/BF	83,000	933	4,474	17,258	12,464	7,159	11,772	5,262
	M_Y	OWS/SAS/BF	35,000	336	498	981	1,875	1,130	1,720	1,661
	M_Z	OWS/SAS/BF	28,700	600	1,513	3,267	2,678	2,750	3,461	1,933
	M_X	OWS/SAS/PR	1,000	2	14	35	33	21	30	18
	M_Y	OWS/SAS/PR	17,000	154	318	445	870	479	882	839
	M_Z	OWS/SAS/PR	26,350	79	591	1,200	1,061	1,441	1,788	1,809
	THETAX			.001	.016	.022	.036	.032	.044	.029
	THETAY			.001	.010	.057	.033	.021	.038	.013
	THETAZ			.000	.010	.042	.021	.017	.031	.011

* Moments in in-lb, angles in deg.

† Most significant entry in the table.

tunnel regardless of bending. The static load due to any one jet has a constant value while the jet is on and is zero while the jet is off. The dynamic load is a function of the state of the bending modes. In general, after any of the bending modes has been excited, the dynamic load will vary with time, often having the appearance of a damped sinusoid or the sum of sinusoids of different frequencies.

Because the largest ratio of observed load to assumed load limit occured about the X axis at the CSM/MDA, maximum static, dynamic and sum values are shown for this axis in Table 7. For the Y and Z axes at the CSM/MDA, only the maximum sum values are shown.

For the other load points, the supplied data implicitly makes the assumption that the static loading is relatively small and is thus not simulated. The Table 7 entries for these points are thus maxima for dynamic loads.

In analyzing the data presented in Table 7, obviously the first things to look at are the places singled out in Table 5 as places where high loads might occur. One of the sensitive load points is the Y axis at the OWS/SAS Panel Root load point. The largest observed load here was 882 in-lb which is only about 5% of the assumed load limit of 17,000 in-lb. A second sensitive load point is Z axis at the OWS/SAS Beam Fairing. Here the largest observed load was 3461 in-lb which is about 12% of the assumed load limit of 28,700 in-lb. The simulations thus show that although theoretical considerations indicate that these two places might exhibit high loading if the bending modes are excited at resonance, DAP activity that is typical and representative of real maneuvers produces loads that are a small fraction of the load limits for these points. It can be expected then that during SKYLAB missions, the loading at these two points will cause no problem.

The remaining entry in Table 5 is the X axis at the CSM/MDA. Looking at the line of data for total M_X at the CSM/MDA, we see that CASE 5 shows an observed maximum of 72,470 in-lb. Since the load limit for that point is 88,000 in-lb, the observed load is a significant percentage of the limit. Consequently we cannot casually dismiss this point from further consideration.

Before getting more deeply involved in discussion of M_X at the CSM/MDA, let us cover all the rest of the loads in Table 7. That can be done by observing that of all the entries other than for CSM/MDA M_X, the highest observed load-to-load-limit ratio is the M_X at the OWS/SAS Beam Fairing for CASE 3. The observed load is 17,258 in-lb or about 21% of the load limit. Based on the above observation and all the discussion so far in this and previous sections, it is reasonable to conclude that except for M_X at the CSM/MDA, loads produced during all types of DAP maneuvers and under the full range of disturbances are a small percentage of the load limits.

It is interesting that although the ATM solar arrays look as if they might be the most delicate part of the Orbital Assembly, both the worst-case analysis and the results of simulations recorded in Table 7 indicate that the loads that can be expected to occur at the ATM/SAS will be a very small percentage of the load limits at that point.

What remains to be discussed is M_X at the CSM/MDA. In none of the cases documented in Table 7 does the observed load exceed the assumed load limit of 88,000 in lb. However, in several of the cases the observed load reaches a sufficiently large percentage of the load limit (83% for CASE 4) that some more detailed consideration is called for.

To avoid possible confusion, it should be noted that total M_X is the sum of the signed values of static and dynamic M_X, which explains why the maximum magnitude of the sum can be less than the maximum magnitude of static M_X or dynamic M_X as, for example, in CASE 1.

In considering the CSM/MDA M_X data of Table 7, it should be remembered that CASES 4, 5, 6 and 7 all involve on-failures of an RCS jet. CASES 1, 2 and 3 and the parts of CASES 4, 5, 6 and 7 prior to the failure exhibit loads less than 40,000 in-lb. This leads to the generalization that the normal non-failure operation will result in lower loads than operation during a jet on-failure.

The four on-failure cases are intentionally very similar, differing one from the next in one essential feature. In CASE 4, +X translation is

initiated at 20 seconds. At 40 seconds jet 15 is forced to fail on. Figure 8 shows the jet activity and Fig. 9 shows the total M_X during the run. Figure 8 indicates that it takes about 3 seconds for the vehicle to be pushed to the edge of the roll deadband. At about 43 seconds, jets 14 and 16 begin to pulse to counteract the + roll disturbance of the failed-on jet 15. At about 45.8 seconds combined roll and pitch firings commence as evidenced by the start of jets 9, 11, and 14 pulsing. The online edit program designates 45.105 as the time at which the maximum total M_X occurs.

Figures 10 and 11 are the jet activity and total M_X plots for CASE 5. In CASE 5 the bending mode damping ratio has been set to 0.01. In CASE 4 and in all other simulations except those where there is an explicit statement to the contrary, the MIT all-digital simulator uses a damping ratio of 0.005. The bending data received from Martin Marietta predicts the damping ratio for the bending modes to be 0.01 $\pm$ 0.005. A damping ratio from the low end of the predicted range was used because the smaller the damping ratio, the larger the potential resonant response. Use of the 0.005 damping ratio thus should result in a conservative simulation that can be expected to exhibit more severe bending behavior than would be exhibited with damping ratios that are closer to the predicted mid-range value, 0.01.

Comparison of the CASE 5 results with the CASE 4 results shows that the loads for the case with the higher damping ratio are lower in most instances. This same observation applies to pairs of simulations differing in damping ratio that were run on older bending and vehicle mass-property data but whose results are not specifically enumerated in this memo. Of greatest interest at the moment, is the fact that whereas the total M_X in CASE 4 peaked at 72,470 in-lb, the maximum total M_X in CASE 5 was considerably less, 47,439 in-lb.

It is quite possible that some or many of the bending modes will, in reality, have an actual damping ratio of 0.01 or more. There is thus reason to expect that actual loads occurring during SKYLAB missions will be lower than the values predicted by simulations run with the damping rates set to 0.005.

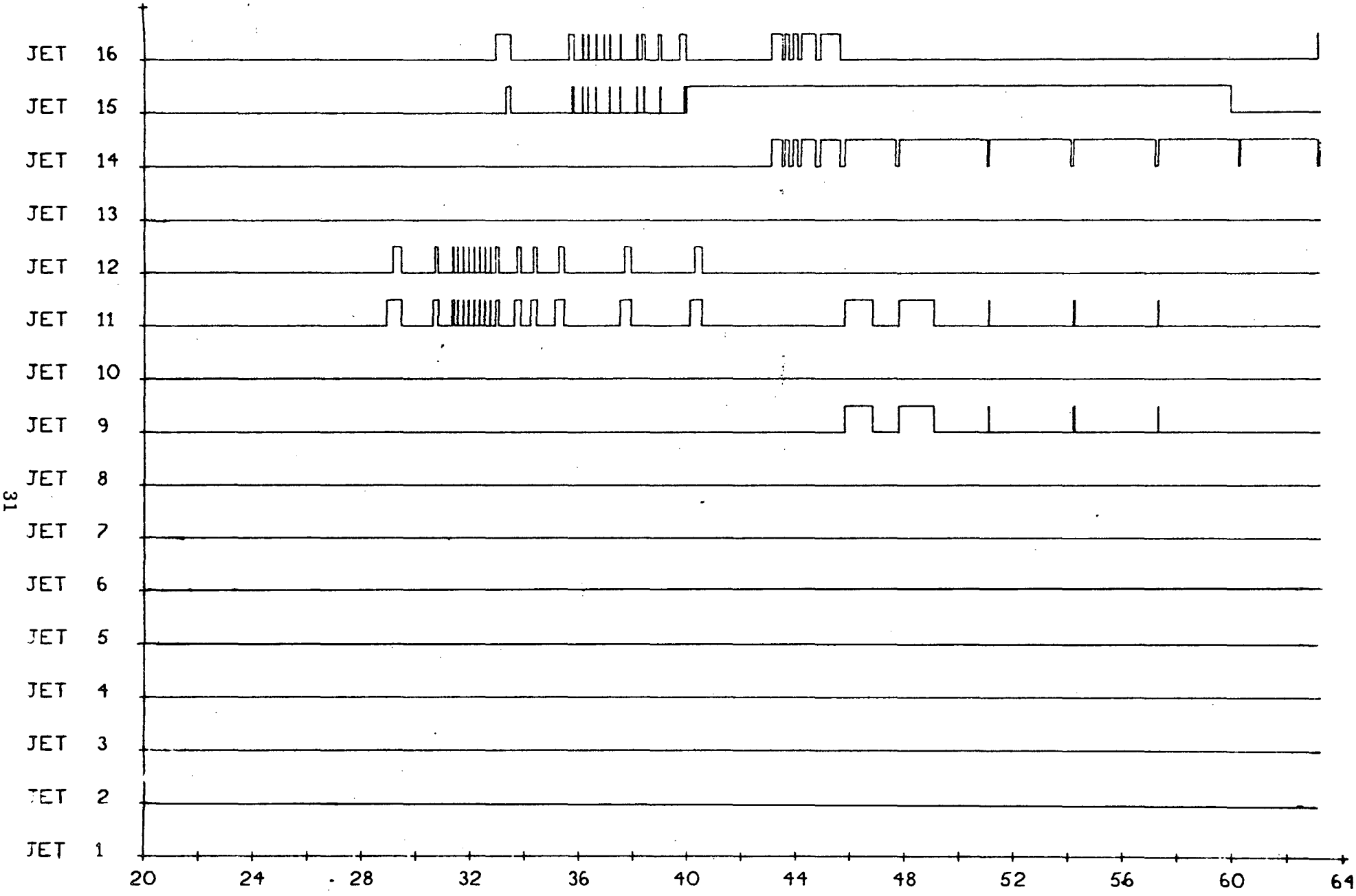

Fig. 8 Jet-firing History for Case 4

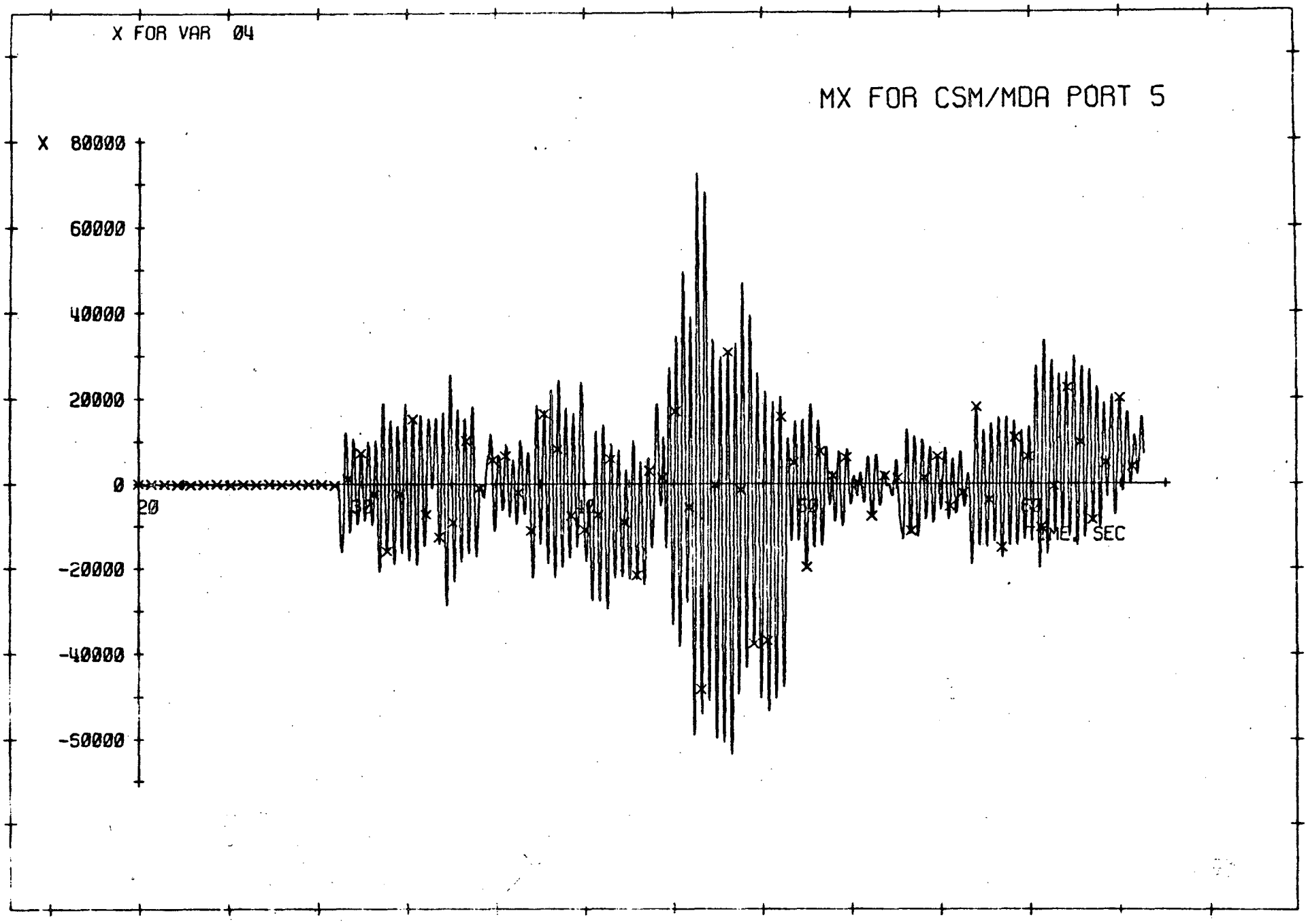

Fig. 9 Total M_X History for Case 4

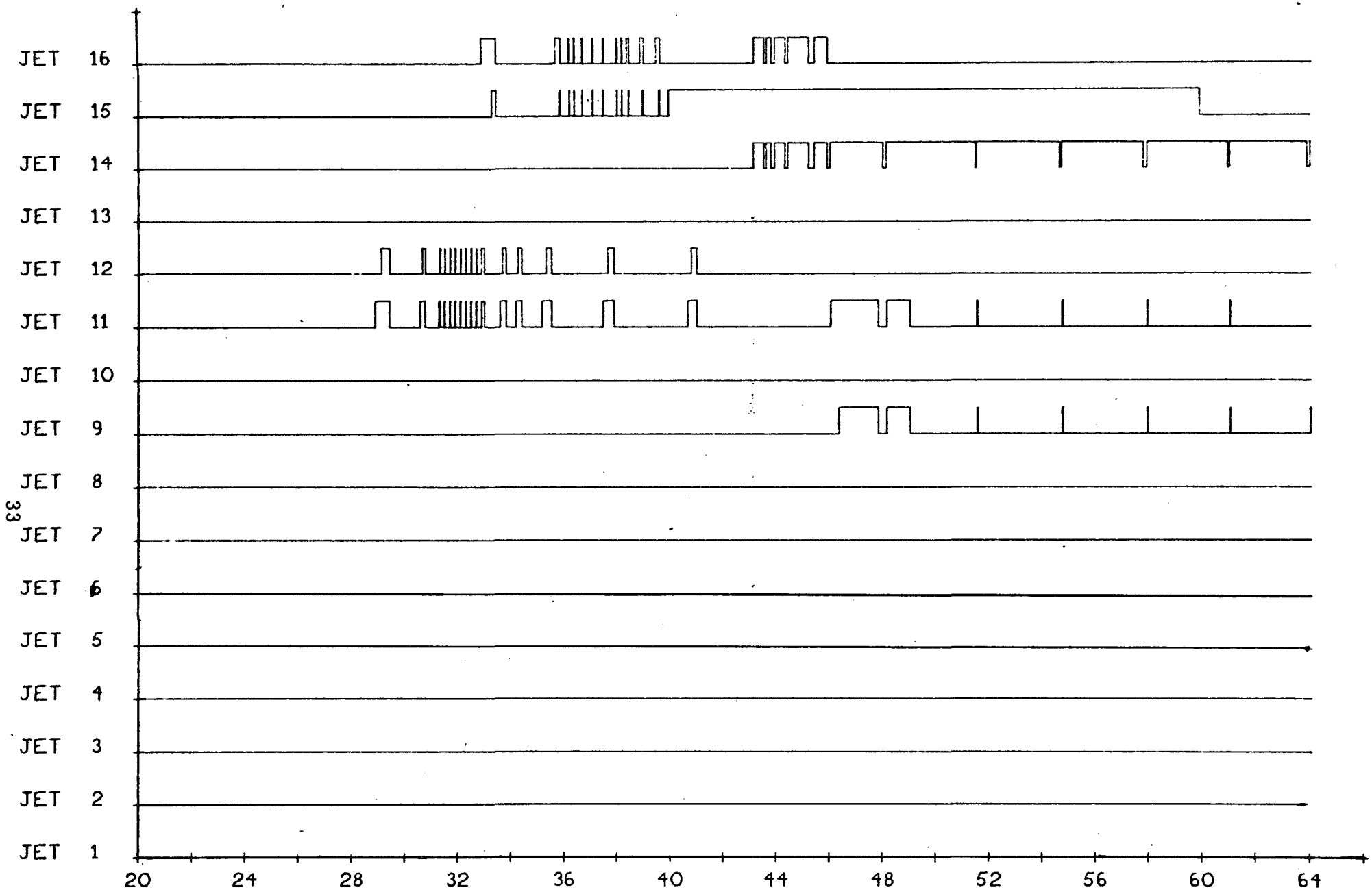

Fig. 10 Jet-firing History for Case 5

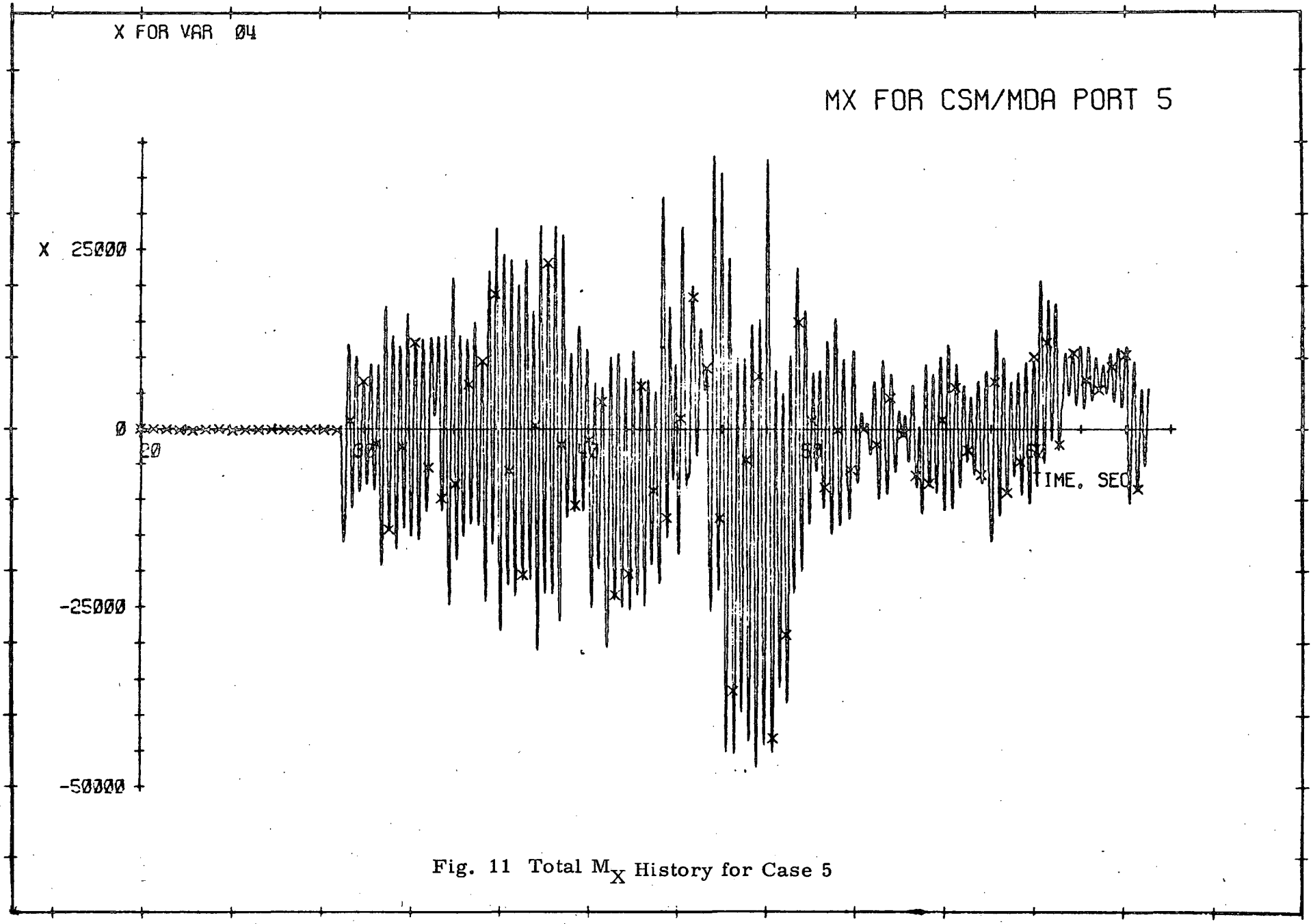

Fig. 11 Total M_X History for Case 5

CASE 6 differs from CASE 4 by the values loaded for the DAP erasable memory constants. * The constants used in CASE 4 were calculated as a function of a set of mass-property data that modeled a vehicle that was somewhat lighter than the vehicle that was actually being simulated by the MIT all-digital simulator. The constants for CASE 6 were computed as functions of a set of mass properties that more closely approximate those of the vehicle actually being simulated.

In CASE 4 the DAP "thinks" the vehicle is lighter than it actually is, with the result that the DAP gains† are lower than nominal. This means that any given firing will be a little too short. The gains that are part of the set of DAP constants used for CASE 6 are somewhat higher. In general, it can be expected that for a vehicle whose mass properties are fixed, use of higher DAP gains will, when the DAP is counteracting a disturbance torque, result in fewer firings each of which is a little longer than would be the situation if lower gains were used. It is theorized that reduction of jet activity in this way may also reduce the loads included at the CSM/MDA. The fact that the maximum M_X load in CASE 6 is about 6,600 in-lb less than in CASE 4 tends to support this hypothesis.

CASE 7 is essentially the same as CASE 6 except that no X translation is included in CASE 7. All CASE 7 is intended to prove is that the effects of a jet-on failure are of the same order of magnitude whether or not it occurs during X translation. Comparison of the CASE 6 and 7 results shows that this is true.

Going beyond simply picking off the peak load during a run it is informative to look at the overall load history. In Figs. 9 and 11, there are usually 29, 30 or 31 positive peaks in any 10 second interval. Therefore the predomenant frequency associated with the M_X loads at the CSM/MDA is about 3 cps. This should come as no surprise since the worst-case study indicated that it is the bending mode whose

---

* These are constants in the sense that they generally do not vary with time. They are not, however, hard wired into the computer and so can be updated or changed from time to time by either ground or astronaut action.

† The so called DAP gains are a subset of the erasable memory constants. The product of the "gain" times the desired rate change gives the jet on-time needed to execute the desired rate change.

frequency is modeled as 2.966 cps that is most likely to produce high loads at the CSM/MDA interface. The simulations thus bear out this conclusion of the worst-case study.

It is also worthwhile discussing what kind of jet activity, in a qualitative sense, caused the high loads in CASE 4. The maximum value of total M_X in CASE 4 occurred at 45.105 sec. Looking at Fig. 8 again we see that the peak load occurred while jet 15 was on continuously and near the end of a sequence of jet 14 and 16 firings. The firings are of moderate duration separated by moderate or short off-times. With jet 15 on, there is a net one-jet plus-roll torque being applied. When jets 14, 15 and 16 are all on together, there is a net one-jet minus-roll torque. The exciting function can be broadly characterized as a few cycles of a square-shaped wave with a non-uniform half period and a peak-to-peak torque amplitude of two roll-jets centered about zero.

Earlier in the run (28-40 seconds), there is a considerable amount of jet activity. Jets 11 and 12, when on simultaneously, are a -Z force pair which will produce primarily pitch acceleration. Therefore jets 11 and 12 turning on and off together would not be expected to strongly excite the 2.966 cps mode which is primarily a torsional mode. However, in almost all of the firings between 28 and 40 seconds, jet 11 turns on before jet 12. This is true even for the very short pulses where the difference in on-times of jet 11 and jet 12 may not be apparent in Fig. 8. While jet 11 is on alone there is a net + one roll jet torque. With 11 and 12 both on the net roll torque is zero. During much of the interval between 28 and 40 seconds, there is an exciting function that can be characterized as a square-shaped wave with a non-uniform half period and a peak-to-peak torque amplitude of one roll-jet centered about a + 1/2 roll jet torque. The load prior to the jet failure remains less than 30,000 in-lb. This seems to indicate that sheer numbers of firings is not of prime significance in producing loads.

Figure 12 is the jet firing history for CASE 1. This simulation of attitude hold against a gravity gradient level disturbance torque resulted in 18 very short jet firings. The loads produced are relatively small. CASE 2, which is the attitude maneuver simulation, produced

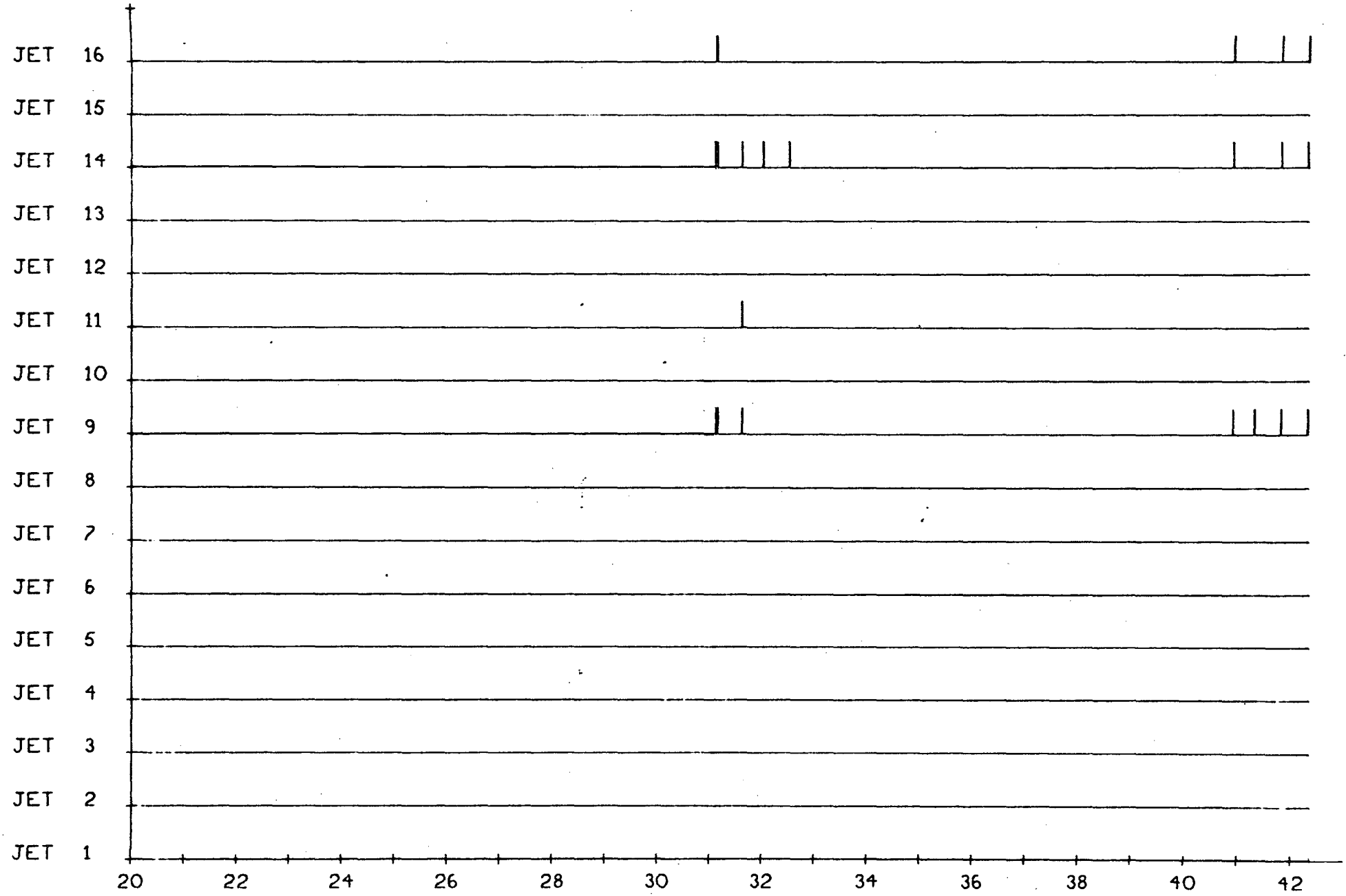

Fig. 12 Jet-firing History for Case 1

12 firings (see Fig. 13). The loads in CASE 2 were much higher than in CASE 1. An obvious difference in the firing patterns is that some of the CASE 2 firings are of substantial duration. The fact that these firings produce higher loads can be made to seem reasonable by the following argument. It is the step change in jet thrust that is the source of bending excitation. For very short firings the effect of the on-step is almost cancelled by the effect of the off-step. Quantitatively the 14 ms minimum impulse time is only 4% of the 2.966 cps mode's period.

This discussion combined with the previous discussion of the type of jet activity in CASE 4 encourages us to make the generalization that a few moderate duration pulses are probably the worst type of excitation that will be experienced by the Orbital Assembly. Contrary to the expectation held by many prior to the simulation study, strings of minimum impulses do not appear to be a severe bending excitation.

A few words specifically directed towards static loads is perhaps appropriate. Static M_X loads occur roughly in multiples of 7500 in-lb. Two is the largest multiple observed in the cases recorded in Table 7. This multple of two occurs when two roll jets of the same sign are firing simultaneously. The design of the Docked DAP makes it possible for three roll jets of the same sign to fire simultaneously when executing combined commands. This occurrence would result in a static M_X of roughly 22,500 in-lb. The largest dynamic M_X in Table 7 is 66,500 for CASE 4. If these two loads were to occur at the same time and have the same sign the total M_X would be 89,000 in-lb or 1,000 in-lb over the limit. This, however, is compounding pessimism with pessimism. The fact that we have to go to such lengths to hypothesize a case that would exceed the load limit should be a reassurance that we can, with a high degree of confidence, expect the load produced by DAP activity to remain below the load limits.

Emphasis until now has been on maximum loads. Taking a slightly different point of view, we note that the auto maneuver of CASE 2 resulted in a peak load of 27,824 in-lb. Glancing again at

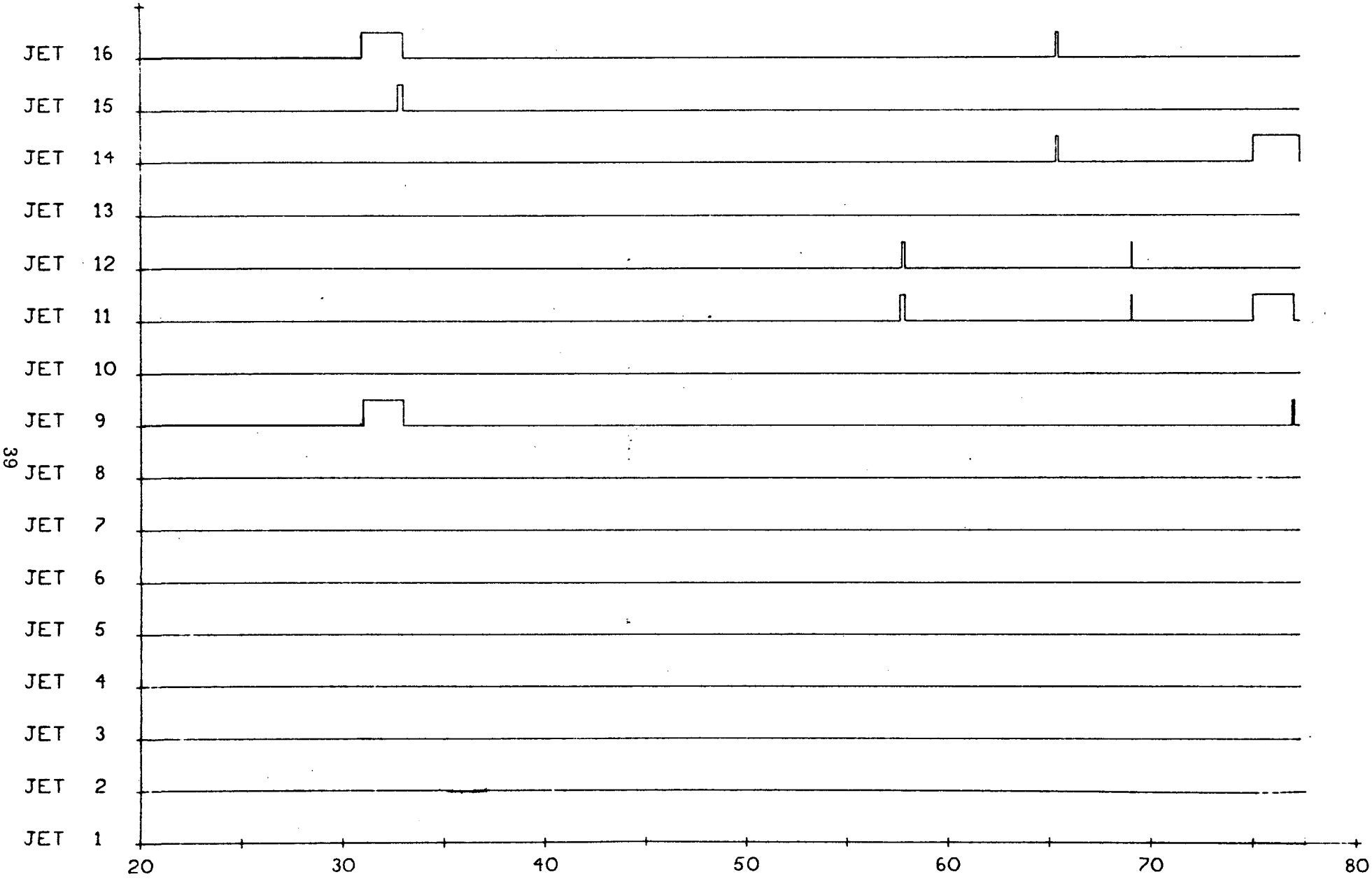

Fig. 13 Jet-firing History for Case 2

Fig. 13, it is obvious that the amount of jet activity in this case is just about minimal. From this we conclude that even for the simplest DAP maneuvers, M_X loads of about 30,000 in-lb can be anticipated at the CSM/MDA. CASE 1 where the loads are much lower can't be considered a contradiction to this statement because all the firings in CASE 1 were very short which is not typical. One implication of this is that relative to the loads produced by simple maneuvers, the loads produced in cases of high jet activity (i.e., CASES 4 through 7) are not drastically higher.

VII. Summary and Conclusions

One part of the investigation into DAP/flexible vehicle interaction concentrated on the question of whether bending could feedback through the DAP to a degree sufficient to result in an instability or self-sustained oscillation. Theoretical consideration and simulations indicate that such an instability or self-sustained oscillation cannot occur.

The study of loads produced by DAP activity is not as quickly summarized. The theoretical approach indicated there were three loads that might be high relative to their load limits. These were M_X at the CSM/MDA interface, M_Z at the OWS/SAS Beam Fairing, and M_Y at the OWS/SAS Panel Root. Simulations showed that the latter two loads did not reach significant proportions during simulated maneuvers. M_X at the CSM/MDA was the only load to exhibit a high value relative to its limit. The largest peak load observed was 72,470 in-lb which is still below the assumed load limit of 88,000 in-lb. Of course, of critical importance is the value of the load limit. The conclusions of this report are based on a load limit value of 88,000 in-lb which is the value stated in the Marshall Space Flight Center report, "Cluster Orbital Maneuver Loads" and which, as we understand, contains a safety factor of 1.4. If, however, the load limit were to decrease substantially (15% or more) the conclusions of this report might be invalidated.

There is always the chance that jet activity with slightly different phasing will produce higher loads than those observed in the specific simulations documented in this report. However, there are several considerations that tend to encourage the belief that actual loads will fall below the 72,470 in-lb value rather than above it. First, of course, is the fact that the case that produced the 72,470 in-lb load was a jet on-failure case. Without jet failures, disturbance torques will be much lower and so, most likely, will induced loads. Secondly, a pessimistic value (0.005) for damping ratio was used in the simulation that exhibited the 72,470 in-lb load. The same simulation with a damping ratio of 0.01 resulted in a peak load of 47,439 in-lb. Finally,

---

* Sterett: "Cluster Orbital Maneuver Loads", S & E - ASTN - ADL (71 - 96).

the DAP gains used in the 72,470 in-lb load simulation were somewhat low for the vehicle being simulated. There is indication that use of nominal or somewhat higher than nominal gains will tend to produce fewer control firings each somewhat longer in duration, which, in the cases observed, has resulted in somewhat lower loads.

Two more generalizations can be made on the basis of the material covered in this report. First, despite their fragile appearance, the ATM Solar Arrays do not exhibit high loads at points of attachment to the ATM. Second, the sheer number of jet firings is of little consequence as far as inducing loads is concerned. This is evidenced by the fact that the highest M_X load at the CSM/MDA interface was produced by a few moderately spaced firings of moderate duration.

In overall summary, the investigation of DAP/flexible vehicle interaction has shown that the highest ratio of load-to-load limit can be expected to occur about the X axis at the CSM/MDA interface and that, based on the bending and load limit data available at this time, one can expect that loads will not exceed their limits during any phase of DAP activity. Therefore the DAP, as programmed in SKYLARK I, is suitable for use during all phases of the SKYLAB mission.

Appendix A

Linear Analysis of SKYLAB Bending for Square Wave RCS-jet Input

Quantities of Interest

The quantities of interest in the linear worst-case analysis are the steady-state bending-induced rotational deflections (peak-to-peak amplitude) at the CSM IMU location and moment loads (peak amplitude) at specific stations due to a square wave input corresponding to a single RCS-jet pulsing on and off at the resonant frequency of each particular mode. The deflections and loads at any instant of time for an arbitrary input may be expressed as the product of a transformation factor with an appropriate derivative of the generalized bending coordinate, as shown in the remainder of this section. Specialization to the steady-state amplitudes of these quantities for an input which approximates a square wave is developed in the next section.

The bending deflection of SKYLAB can be expanded in terms of an infinite number of orthogonal eigenfunctions (modes) and their associated eigenvalues (frequencies). The external excitations (forcing functions) driving these modes, when expanded in terms of the same eigenfunctions, may be formed as the vector inner product of the external force and the normalized deflection of the mode at the point of application of the force. For the Lth particular mode, then, the equation of motion of the generalized bending coordinate may be written as:

$$\ddot{q}_L + 2\zeta_L \omega_L \dot{q}_L + \omega_L^2 q_L = f_L(t) \qquad \text{(A-1)}$$

where q_L is the bending coordinate, ω_L is the natural frequency, and ζ_L is the damping ratio. The forcing function for the Lth mode is:

$$f_L(t) = \sum_J (\bar{D}_{J,L} \cdot \bar{F}_J)/GM \qquad \text{(A-2)}$$

where $\bar{F}_J$ is one of the contact forces which excite bending, $\bar{D}_{J,L}$ is the normalized deflection of the Lth mode at the point of application of $\bar{F}_J$, and GM is the generalized mass.

The rotational deflection of the navigation base for each mode is the product of the modal displacement vector at the navigation base ($R\bar{N}B$) and the generalized bending coordinate:

$$\bar{\theta}_L = R\bar{N}B_L \, q_L \tag{A-3}$$

The vector moment (load) at station K due to bending is given by the product of the modal-acceleration loads transformation matrix ($\overset{*}{MLT}$) and a vector composed of the second derivative of the bending coordinates for each mode:

$$\bar{M}_K = \overset{*}{MLT}_K \left\{ \begin{array}{c} | \\ \ddot{q}_L \\ \downarrow \end{array} \right\} \tag{A-4}$$

The quantities of interest in the worst-case analysis are given by Eqs. (A-3, 4) when the values of q and $\ddot{q}$ substituted into these equations correspond to the amplitudes of the steady-state oscillations obtained from single-jet excitation by each RCS-jet of each significant bending mode separately at the resonant frequency of the mode. The following section describes a method for computing the steady-state q and $\ddot{q}$ amplitudes analytically for a periodic input which approximates the bending excitation due to a single jet pulsing on and off at the resonant frequency of the particular mode.

Steady-state Response of the Bending Coordinate

This section derives an expression for the output of one of the second order bending equations (A-1) corresponding to a square wave input. The solution is initially expressed as a sum of sinusoids at integer multiples of the modal frequency, but it is shown that the contributions of the higher frequency harmonics to the output signal are negligible compared to the fundamental frequency component. Retention of just the d. c. and fundamental terms

in the output signal simplifies analysis.

For any particular mode, Eq. (A-1) may be written as:

$$\ddot{q} + 2\zeta\omega\dot{q} + \omega^2 q = f(t) \qquad \text{(A-5)}$$

The driving term is assumed to stem from the Jth single jet pulsing on and off at the resonant frequency of the mode; thus the input $f(t)$ may be represented as a square wave with period

$$T = 2\pi/\omega \qquad \text{(A-6)}$$

and amplitude

$$AMPJ = (\bar{D}_J \cdot \bar{F}_J)/GM \qquad \text{(A-7)}$$

where the index J refers to any particular one of the 16 RCS jets. The input $f(t)$ is plotted for an appropriate phase angle in Figure A-1.

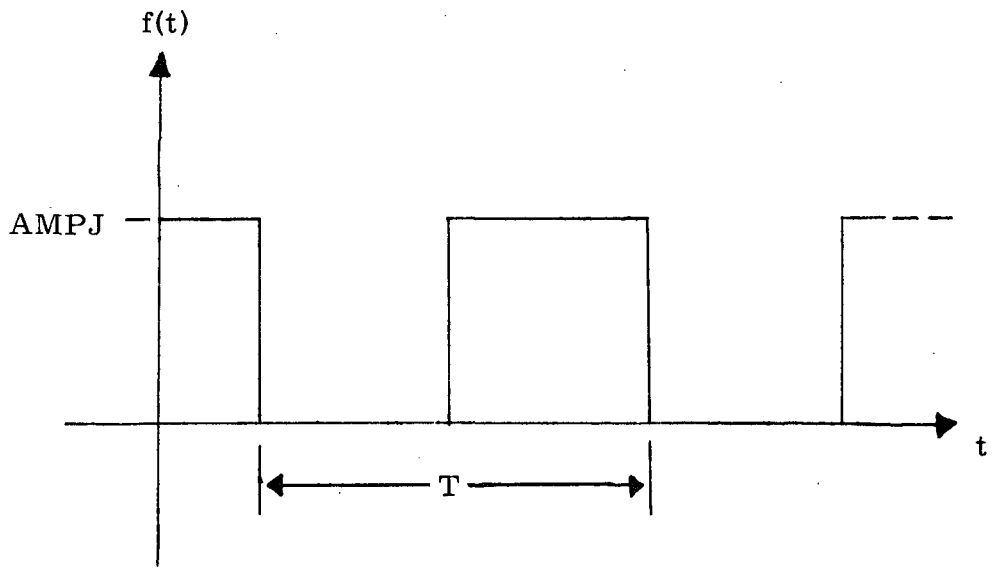

Figure A-1 Excitation to Bending Equation (A-5) for the Jth RCS-jet Pulsing at Resonance

It is convenient now to expand f(t) in a Fourier series, i.e. to express f(t) as

$$f(t) = \frac{a_0}{2} + \sum_{n=1}^{\infty} (a_n \cos n\omega t + b_n \sin n\omega t) \qquad \text{(A-8)}$$

where

$$a_n = \frac{2}{T} \int_0^T f(t) \cos n\omega t \, dt$$

$$b_n = \frac{2}{T} \int_0^T f(t) \sin n\omega t \, dt \qquad \text{(A-9)}$$

$$a_0 = \frac{2}{T} \int_0^T f(t) \, dt$$

Putting f(t) from Figure A-1 into the coefficient expressions Eqs. (A-9) one obtains:

$$a_n = \begin{cases} \text{AMPJ} & n = 0 \\ 0 & n = 2, 4, 6, \ldots \\ \frac{2\,\text{AMPJ}}{\pi n} & n = 1, 5, 9, \ldots \\ -\frac{2\,\text{AMPJ}}{\pi n} & n = 3, 7, 11, \ldots \end{cases} \qquad \text{(A-10)}$$

$$b_n = 0 \qquad n = 1, 2, 3, \ldots$$

Equations (A-8) and (A-10) may now be used to write f(t) in the compact form:

$$f(t) = \frac{\text{AMPJ}}{2} + \frac{2\,\text{AMPJ}}{\pi} \sum_{k=0}^{\infty} \frac{(-1)^k}{(2k+1)} \sin\left([2k+1]\,\omega t + \frac{\pi}{2}\right) \qquad \text{(A-11)}$$

The output of a system of the form given in Eq. (A-5) to an input of the form given in Eq. (A-11) is:

$$q(t) = \frac{p_0}{2} + \sum_{n=1}^{\infty} A_n \sin(n\omega t - \alpha_n) + \text{transient} \tag{A-12}$$

For the case in question, the following relations hold regarding Eq. (A-12):

$$p_0 = \frac{AMPJ}{\omega^2} \tag{A-13}$$

$$A_n = \begin{cases} 0 & n = 0, 2, 4, \ldots \\ \dfrac{2AMPJ}{\omega^2 n}\left[\left(1-n^2\right)^2 + \left(2n\zeta\right)^2\right]^{-1/2} & n = 1, 5, 9, \ldots \\ \dfrac{2AMPJ}{\omega^2 n}\left[\left(1-n^2\right)^2 + \left(2n\zeta\right)^2\right]^{-1/2} & n = 3, 7, 11, \ldots \end{cases} \tag{A-14}$$

$$\alpha_n = \frac{\pi}{2} + \tan^{-1}\left(\frac{2n\zeta}{1-n^2}\right) \qquad \left(\frac{\pi}{2} < \alpha_n < \frac{3\pi}{2}\right) \tag{A-15}$$

Neglecting the transient term in Eq. (A-12), this equation may be used along with Eqs. (A-13, 14, 15) to write the steady-state bending coordinate response (q_{ss}) in compact form:

$$q_{ss} = \frac{AMPJ}{2\ 2} + \sum_{k=0}^{\infty} (-1)^k A_k \sin\left[(2k+1)\omega t - \alpha_k\right] \tag{A-16}$$

where

$$A_k = \frac{AMPJ}{\pi\omega^2(2k+1)}\left[4(k^2+k)(k^2+k+\zeta^2) + \zeta^2\right]^{-1/2} \tag{A-17}$$

$$\alpha_k = \frac{\pi}{2} + \tan^{-1}\left(-\frac{(2k+1)\,\zeta}{2k\,(k+1)}\right) \qquad \text{(A-18)}$$

It is now shown that neglecting terms for $k \geq 1$ in Eq. (A-16) yields a very good approximation for q_{ss}. Noting that $\zeta = .005$ is negligible compared to k for $k \geq 1$, one deduces

$$A_k \approx \frac{AMPJ}{2\pi\omega^2 k\,(2k+1)\,(k+1)} \quad ; \quad k \geq 1 \qquad \text{(A-19)}$$

This expression yields

$$A_1 \approx \frac{1}{12}\,\frac{AMPJ}{\pi\omega^2} \qquad \text{(A-20)}$$

Terms for $k > 1$ can be seen from Eq. (A-19) to have magnitude less than A_1. The $k = 0$ term, however, is given by

$$A_0 = \frac{1}{\zeta}\,\frac{AMPJ}{\pi\omega^2} = 200\,\frac{AMPJ}{\pi\omega^2} \qquad \text{(A-21)}$$

Since A_0 is seen to be larger in magnitude than A_1 and subsequent terms by at least a factor of 2400, the neglect of terms corresponding to $k \geq 1$ is justified.

Retaining only the $k = 0$ term in the summation in Eq. (A-16), then, one obtains:

$$q_{ss} \approx \frac{AMPJ}{2\omega^2} + \frac{AMPJ}{\pi\zeta\omega^2}\sin(\omega t - \pi) \qquad \text{(A-22)}$$

Approximate expressions for the first two time-derivatives of q_{ss} are seen

to be:

$$\dot{q}_{ss} \approx \frac{AMPJ}{\pi \zeta \omega} \cos(\omega t - \pi) \tag{A-23}$$

$$\ddot{q}_{ss} \approx -\frac{AMPJ}{\pi \zeta} \sin(\omega t - \pi) \tag{A-24}$$

Finally, the quantities of interest in the worst-case analysis are obtained. The peak-to-peak rotational deflection is given by Eq. (A-3) when for q_L is substituted the quantity

$$\left| q_{ss} \right| = \frac{AMPJ}{\pi \zeta \omega^2} \tag{A-25}$$

and the peak moment loads at station K is given by Eq. (A-4) when for each $\ddot{q}_L$ is substituted the quantity

$$\frac{1}{2} \left| \ddot{q}_{ss} \right| = \frac{AMPJ}{2 \pi \zeta} \quad . \tag{A-26}$$

Appendix B

Fourier Analysis for Pulse-train Input

This appendix develops an approximate formula for the output amplitude reduction factor obtained when the input to one of the bending equations (A-5) is a pulse train at period $2\pi/\omega_n$ rather than a true square wave; i.e., a jet is "on" for $\chi T/2$ and "off" for $(2-\chi)T/2$ rather than both "on" and "off" for $T/2$ as in Figure A-1. As in Appendix A, all harmonics above the fundamental are neglected.

For the case considered, the Fourier coefficients (Eq. (A-9)) become

$$a_n = \frac{AMPJ}{\pi} \sin \chi n \pi$$

$$b_n = \frac{AMPJ}{\pi} (1 - \cos \chi n \pi) \qquad \text{(B-1)}$$

$$a_0 = AMPJ\ \chi$$

Retaining only terms for $n \leq 1$, the input to one of the bending equations may be written as

$$\tilde{f}(t) = \frac{AMPJ\ \chi}{2} + \frac{AMPJ \sin \chi \pi}{\pi} \cos \omega t + \frac{AMPJ\,(1-\cos \chi \pi)}{\pi} \sin \omega t$$

$$= \frac{AMPJ\ \chi}{2} + \frac{2\ AMPJ}{\pi}\ \tilde{\chi}\ \sin(\omega t - \tilde{\beta}) \qquad \text{(B-2)}$$

where

$$\tilde{\chi} = \frac{1}{2}\left[(\sin \chi \pi)^2 + (1-\cos \chi \pi)^2 \right]^{1/2}$$
$$= \frac{\sqrt{2}}{2} (1-\cos \chi \pi)^{1/2} \qquad \text{(B-3)}$$

$$\tilde{\beta} = \tan^{-1}\left(\frac{1-\cos \chi \pi}{\sin \chi \pi} \right) \qquad \text{(B-4)}$$

Comparing Eqs. (B-2) and (A-11) for $k = 0$ (i.e., $n = 1$) determines that the ratio of the amplitudes of the input sinusoids is just $\tilde{\chi}$. Following the developments of Appendix A, it is clear that the bending coordinate acceleration magnitude $(\ddot{\tilde{q}}_{ss})$ for $\tilde{f}$ input will be in this same proportion to $|\ddot{q}_{ss}|$ in Eq. (A-26). Thus, the sought amplitude reduction factor is:

$$\frac{|\ddot{\tilde{q}}_{ss}|}{|\ddot{q}_{ss}|} = \frac{\sqrt{2}}{2} (1-\cos \chi \pi)^{1/2} \qquad \text{(B-5)}$$

DISTRIBUTION LIST

Internal:

R. Bairnsfather
R. Battin
N. Brodeur
T. Chan
S. Copps
D. Corwin
S. David
L. Drane
G. Edmonds
R. Gilbert
K. Glick
J. Goode
K. Goodwin
K. Greene
M. Hamilton
R. Haslam
D. Hoag
J. Jones
R. Kiburz
K. Kido
B. McCoy
H. McOuat
V. Megna
H. Nayar
W. Ostanek
P. Rye
G. Silver
L. Silver
G. Stubbs
J. Turnbull (10)
F. Walsh
R. Werner
R. White
C. Work
Apollo Library (2)
MIT/DL TDC (10)

External:

MSC: (29&1R)

National Aeronautics and Space Administration
Manned Spacecraft Center
Houston, Texas 77058
ATTN: Apollo Document Control Group (BM86) (18&1R)
K. Cox EG2
J. Garman FS6
T. Gibson
E. Kubiak
T. Lawton EG/MIT
T. Lins EG2
G. Sabionski FS661 (2)
P. Shaffer FC5
H. Tindall FM
C. Sykes FS6

Bernie Suchocki (4)
CFK/Flight Crew Operations Branch
Flight Crew Training Bldg. (M7-409)
Kennedy Space Center

R. C. Schoen DA35
NAR Corporation, Space Division
12214 Lakewood Blvd.
Downey, California 90241

J. D. Williams
Lockheed Electronics Co., Inc.
Houston Aerospace Systems Division
16811 El Camino Real
Houston, Texas 77058
Mail Code C32

Jack Heybl (2)
Delco Electronics Division, GMC
Milwaukee, Wisconsin
Dept. 2A09

R. A. Heath (5)
Mail No. E8843
Martin Marietta Corporation
PO Box 179
Denver, Colorado 80201

R. D. Miller (3)
H4-2018
TRW Systems Houston Operations
Space Park Drive
Houston, Texas 77058